Australian Government
Bureau of Meteorology

The Centre for Australian Weather and Climate Research
A partnership between CSIRO and the Bureau of Meteorology

CSIRO

Evaluation and implementation of AUSWAVE

Tom Durrant and Diana Greenslade

CAWCR Technical Report No. 041

September 2011

www.cawcr.gov.au

Evaluation and implementation of AUSWAVE

Tom Durrant and Diana Greenslade

The Centre for Australian Weather and Climate Research
- a partnership between CSIRO and the Bureau of Meteorology

CAWCR Technical Report No. 041

September 2011

ISSN: 1836-019X

National Library of Australia Cataloguing-in-Publication entry

Author: Tom Durrant and Diana Greenslade

Title: Evaluation and Implementation of AUSWAVE

ISBN: 978-1-921826-61-0 (PDF/Electronic Resource)

Series: CAWCR technical report; 41

Subjects: Climatology--Mathematical models.

Numerical weather forecasting--Australia—Mathematical models.

Meteorology--Mathematical models

Ocean-atmosphere interaction—Australia--Simulation methods.

Notes: Included bibliography references and index

Other Authors / Contributors: Day, K.A. (Editor)

Dewey Number: 551.63

Enquiries should be addressed to:
Tom Durrant
Centre for Australian Weather and Climate Research:
A partnership between the Bureau of Meteorology and CSIRO
GPO Box 1289, Melbourne
Victoria 3001, Australia

t.durrant@bom.gov.au

Copyright and Disclaimer

Contents

List of Figures

List of Tables

ABSTRACT

The Bureau of Meteorology has run a version of the WAM model, AUSWAM, for the past 15 years. The recent significant changes to the forcing winds with the implementation of the Australian Community Earth System Simulator (ACCESS) system has prompted the evaluation of the WAVEWATCH III® model as a possible replacement.

The implementation of WAVEWATCH III® within the Bureau of Meteorology's forecasting environment is known as AUSWAVE. This report documents the testing and verification of the AUSWAVE model. The benefits that this model offers over AUSWAM are described and the error characteristics of both models are compared.

A number of hindcasts are performed over a four month period from July to October 2008. Verifications are carried out against both altimeter data and buoy data around the Australian coast, with the aim of identifying the most suitable configuration for the Australian region. This set up is then compared with AUSWAM.

AUSWAVE is found to provide clear and immediate improvements over the AUSWAM model, showing forecast skill gains of 36 h to 48 h lead time for significant wave height. A negative bias is present in AUSWAVE. This is due primarily to a low bias in the ACCESS.

1. INTRODUCTION

Wind-generated ocean waves are almost always present at sea. These waves are generated by winds somewhere on the ocean, be it locally, so called wind sea, or thousands of kilometres away, referred to as swell. These waves affect a wide range of activities such as shipping, fishing, recreations, coastal and offshore industry, coastal management and pollution control. They are also important in weather and climate processes as they play a large role in exchanges of heat, energy, gases and particles between the ocean and the atmosphere.

Numerical wave modelling plays an important role in the provision of marine wave forecasts at the Australian Bureau of Meteorology (Bureau). Until 19 August 2010, the Bureau ran a version of the third-generation wave model WAve Model (WAM; WAMDIG, 1988) operationally, known as Australian WAve Model (AUSWAM) (NMOC, 1994). Forecasts of sea-state from AUSWAM were used as numerical forecast guidance for the Bureau's marine services.

In recent years, the performance of AUSWAM had fallen behind that of other overseas model guidance, in part, due to the quality of the surface winds from the Bureau's systems. In late 2010, National Meteorological and Oceanographic Centre (NMOC) replaced all the existing operational Numerical Weather Prediction (NWP) systems (e.g. Global ASsimilation and Prediction System (GASP) (Seaman et al. 1995), Limited Area Prediction System (LAPS) (Puri et al. 1998)) with the new Australian Community Climate Earth System Simulator (ACCESS) system, which is based on the UK Met Office Unified Model/Variational Assimilation (UM/VAR) system (Rawlins et al. 2007). This led to better skill in standard NWP skill scores (NMOC, 2010), including surface winds.

These recent significant changes to the forcing winds meant that the wave model needed to be “re-tuned" to adapt to the new characteristics of the wind forcing. This led to the decision to replace AUSWAM with the more widely-used and computationally-efficient WAVEWATCH III® (WW3) model (Tolman et al. 2002; Tolman 2009).

The implementation of WW3 within the Bureau's forecasting environment is known as AUSWAVE. This report documents the testing and verification of the AUSWAVE model. The benefits that this model offers over AUSWAM are described and the error characteristics of both models are compared. Some background on both AUSWAM and WW3 are given in Section 2, and the model set up, data sources and verification methods are described in Section 3. Results are presented in Section 4 and a summary and conclusion are given in Section 5.

2. BACKGROUND

Wave modelling and computer generated wave forecasting began in the late 1950's (Sverdrup and Munk, 1947; Hubert, 1957) and consisted of rudimentary estimates of a simple wave height and period. A period of rapid wave model development occurred in the 1980's driven by the introduction of the first supercomputers and the promise of a wealth of ocean-surface data from remote sensing instruments. The emergence of the WAM group and the development of spectral models of increasing sophistication saw rapid improvements in operational wave forecasting systems around the world. Reviews of the development of these so called third generation models can be found in (WAMDIG. 1988) and Komen et al. (1996), with more up to date reviews in Tolman et al. (2002) and Janssen (2007).

Numerical wave prediction at the Bureau began with a parametric wave model in 1983, followed by a first-generation spectral model in 1986 (see Greenslade, 2004, for a brief history). Since June 1994, the Bureau has run a version of the WAM model, AUSWAM, which remained in operational use for 15 years (NMOC, 1994). This system is described below in order to provide context for later discussion.

2.1 AUSWAM

The WAM model (WAMDIG; 1988) is a third generation wave model which solves the wave transport equation explicitly without assuming a form for the evolving spectrum. The wave transport equation is:

$$\frac{\partial F}{\partial t} + \nabla(c_g F) = S_{in} + S_{nl} + S_d \qquad (2.1)$$

where $F(f, \theta)$ is the wave spectrum as a function of frequency and direction, c_g is the group velocity and the terms on the right hand side represent the source terms: S_{in} is the energy input due to wind forcing, S_{nl} the non-linear energy transfer between groups of resonant waves and S_d the dissipation of energy due to whitecapping.

The most recent implementation of the WAM model at the Bureau used Cycle 3 physics with increased dissipation and third-order upwinding numerics (Bender and Leslie, 1994; Bender, 1996). Wave spectra were discretised into 24 directional bins, centred at 15°, 45°, 75°, etc. (Durrant et al. 2009b). This ‘staggering’ of the directional bins avoids excessive spectral energy propagating directly along the axes of the north-south co-ordinate system (Bidlot, 1997; Greenslade, 2000). There were 25 frequency bins ranging from 0.0418 Hz to 0.4114 Hz. This represents wave periods ranging from approximately 2.5 seconds to 24 seconds. The propagation and source term time steps were 20 minutes and 10 minutes respectively.

For the global version of the model, the north-south extent of the domain was 78°N to 78°S. Forcing fields for the global wave model were wind velocities at 10 m above sea level. These were obtained from the Bureau’s global atmospheric model, GASP (*Seaman et al.* 1995). Surface winds were obtained from the lowest level of GASP using a physically-based boundary layer model (*Hess et al.* 1995). Sea ice was accounted for indirectly in the model by the use of zero or low wind velocity over areas covered by ice. The ice edge was not included explicitly in the boundaries of the domain.

Altimeter H_s data has been assimilated in the operational model since 2002 (*Greenslade*, 2001; *NMOC*, 2002), with the most recent version assimilating both Jason-1 and Envisat data (*Durrant et al.* 2009b).

AUSWAM has provided high quality marine forecasts over the course of its lifetime at the Bureau. However, the recent upgrade to the atmospheric model, and the release of version 3 of the WW3 model provided strong incentive to examine this model as a possible replacement. Some of the features of WW3 are highlighted below, and discussed in the context of the Bureau's current system, and ongoing operational needs.

2.2 WAVEWATCH III®

WW3 was developed at the National Oceanic and Atmospheric Administration (NOAA) / National Centers for Environmental Prediction (NCEP), where it has been the operational system since 9 March 2000 (Chao et al. 1999). The recently released version 3 of the model has been made freely available by request to NCEP [1]. The description given below is necessarily brief, full details of the model can be found in the user manual and references therein (*Tolman*, 2009).

The prognostic variable used within WW3 is the wavenumber spectrum $F(k,\theta)$, as opposed to the frequency spectrum used by WAM. The wavenumber spectrum is chosen due to its invariance characteristics with respect to physics of wave growth and decay for variable water depths. The WW3 model solves the linear balance equation for the spectral wave action density N in terms of wavenumber k and wave direction θ, as a slowly varying function of space $\mathbf{x}$ and time t:

$$\frac{DN(k,\theta,\mathbf{x},t)}{Dt} = S(k,\theta,\mathbf{x},t) \tag{2.2}$$

This is closely related to the wave transport equation solved within WAM (Equation 2.1), with the action density spectrum N relating to the energy density spectrum F as $N=F/\sigma$, where σ is the intrinsic wave frequency. Similarly, $S = S/\sigma$. The intrinsic frequency is related to the wavenumber through the dispersion relation:

$$\sigma^2 = gk \tanh kd \tag{2.3}$$

where d is the mean water depth. The intrinsic or relative frequency is related to the absolute frequency ω (as observed in a fixed frame of reference) through the Doppler equation:

$$\omega = \sigma + \mathbf{k.U} \tag{2.4}$$

where $\mathbf{U}$ is the mean current velocity vector. The use of the action balance equation in place of the wave transport equation allows for the effect of large scale currents on the evolution of the wave spectrum. In the absence of currents, as is the case in the work presented here, equations2.1 and 2.2 are essentially identical.

Some of the features that make WW3 an attractive option include:

Added physics packages

The source terms are those terms providing input to the evolving spectrum in equations 2.1 and 2.2. In deep water, these consist of S_{in}, S_{nl} and S_d mentioned above. The wind input and dissipation terms are often collectively termed the model 'physics'. The current release of WW3

[1] http://polar.ncep.noaa.gov/waves/wavewatch/wavewatch.shtml

contains a number of different source term options. In addition to the default formulation of Tolman and Chalikov (1996), those of WAM cycles 3 (Snyder et al. 1981; Komen et al. 1984) and 4 (Janssen, 1991) are also available. These are discussed further and tested in section 4.1.1.

Improved Numerics

The so-called ULTIMATE QUICKEST (UQ) numerical scheme used in WW3 is third-order accurate in both time and space, compared to the default first-order scheme of WAM. The Bureau's WAM implementation employed an upgraded third-order numerics scheme, though this introduced some known problems. The impact of the UQ numerics are discussed in section 4.1.2.

Additionally, the use of the fully unsteady spectral action density equation in WW3 enables large-scale wave-current interactions to be taken into account. While ocean surface current forecasting capability is not yet sufficient to warrant inclusion in the operational system, it is likely that the OceanMAPS system (Brassington et al. 2005) will provide this capability in the near future.

Better handling of the Garden Sprinkler Effect (GSE)

The GSE is a numerical feature that is present when the discretization of the spectrum is too coarse for the scale of propagation, causing non-physical discontinuities in the wave field as natural dispersion occurs (e.g.WAMDIG; 1988). In the extreme case, as a swell field propagates, it disintegrates into discrete geographic features, with each feature corresponding to a frequency/direction bin in the model's computational grid. With higher order propagation schemes, the GSE is unfortunately more apparent. Numerical diffusion, though it is an error, has the positive quality of tending to counteract the GSE, smoothing these discrete features together. The upgraded numerics of AUSWAM were known to produce increased occurrences of the GSE. Of course, numerical diffusion in low order numerical schemes is unrelated to physical dispersion and is difficult to control, so it should not be relied upon to mimic the natural dispersion of continuous spectra. Thus, a controllable diffusion was introduced into WW3, in the form of a diffusion correction term to the propagation following Booij and Holthuijsen (1987). In the most recent release, a grid point averaging technique has also been implemented that produces nearly identical results at lower computational cost, particularly at high resolutions (Tolman, 2002b).

Improved spectral partitioning

Wind sea/swell partitioning in AUSWAM, and indeed in WAM in general relies on a reasonably simple relationship between the wind speed and the wave speed. In essence, wind sea is defined as that part of the spectrum which is being actively forced by the wind. The remaining spectrum defines the swell.

There are major limitations to this method of separation. While it can be argued that the separation technique does a reasonable job of separating the wind sea component, averaging what remains into a single swell component is insufficient when the swell component consists of multiple wave systems, as is usually the case, with the resultant output swell indicating a fictitious swell that is the combination of multiple systems. Relying on a wind velocity dependence in order to define the separation also has the drawback that in the event of a rapid wind change, the wind sea/swell separation will change drastically, without any actual change in the wave field itself, which will react far more slowly to these changes.

These deficiencies have been addressed in the latest release of WW3, which now uses the more sophisticated scheme of Hanson and Jensen (2004). Further detail of this scheme can be found in Appendix C. In practice, the biggest change is that instead of outputting a single wind sea and swell, as was the case with AUSWAM, the new model produces wind sea, and a number of swell components. As for WAM, this partitioning is done at every grid point, producing gridded outputs of these fields.

Sub-grid-scale blocking
At the typical resolutions of operational wave models, there are many islands that are too small to be explicitly resolved by the grid. The blocking of wave energy by these unresolved islands and barrier reefs can be a significant source of error in wave prediction models. Accounting for these obstructions explicitly requires high grid resolutions, which are not feasible in an operational environment. Alternatively, such features can be modelled as sub-grid obstructions (Hardy, 2001). This capability has been available in wave models such as SWAN and WW3 for a number of years (Holthuijsen et al. 2002; Tolman, 2003). On a global scale, the impact of sub-grid-scale blocking has been shown to reduce H_s biases in the tropics when compared to ERS-1 data (Tolman, 2003). This capability is of particular relevance in the Australian region, where island chains such as French Polynesia and reef systems such as the Great Barrier Reef are inadequately modelled by explicit techniques.

Dynamical time stepping
As with WAM, WW3 solves the governing equation using a fractional step method, where parts of the equation are solved consecutively. In the case of WW3, divisions include separate calculations for spatial propagation, intraspectral propagation, and source terms. The equations are solved by marching forward in time with an overall global model time step Δt_g, while fractional time steps are allowed to vary depending on the net source term S, a maximum change of action density ΔN and the remaining time in the interval Δt_g, improving both efficiency and accuracy (Tolman, 1992).

Mosaic grids
The mosaic grid approach developed by Tolman (2008) allows two way nesting within WW3. This allows the set-up of a number of telescoping grids to be run in parallel, exchanging information with each other. This approach provides an economical way to locally increase the spatial resolution of the model.

Additionally, grids used either for traditional one-way nests, or as part of a mosaic grid approach can be irregular in shape, unlike the rectangular grids required within AUSWAM. This allows higher resolution grids to conform to coastlines and areas of interest, saving computational resources in areas where they are not needed.

Improved shallow water physics
While the input, non-linear interaction and dissipation terms can adequately model the wave energy in the open ocean, shallow water effects cannot be ignored in coastal regions. AUSWAM did include bottom friction, in the form of the empirical JONSWAP parameterization (Hasselmann et al. 1973). In addition, WW3 includes parametrizations of surf breaking (Battjes and Janssen, 1978) and bottom scattering (Ardhuin and Herbers, 2002).

While these improvements promise to offer substantial improvements over AUSWAM in the coastal zone, for certain applications, specialised models such as SWAN (Holthuijsen et al. 2002) are often required. In addition to the features described above, SWAN also includes triad interactions. Perhaps most critically though, it uses an explicit numerical scheme, as opposed to the semi-implicit scheme used by both WAM and WW3. In the case of the latter models, prohibitively high time-steps are required to maintain numerical stability in high resolution modelling making them unsuitable for this task.

The open, pluggable nature of the WW3 code has resulted in a large growth in the use of this model in the international wave model community, both amongst research groups and operational centres. The code itself has been released under an open source license, with contributions now being made by multiple groups around the world. This has resulted in rapid and continued development of the model. This development is set to continue, with WW3 being at the centre of the recent NOPP project[2], a NOAA / U.S. Navy / U.S Army Core of Engineers (USACE) collaboration funded with approximately $8 million over four years beginning at the start of the 2010 financial year, aiming to develop the next generation wave models.

The version examined in this work is version 3.14. The implementation of this model will not only improve the Bureau's wave forecasting capabilities, but will present significant opportunity for international collaboration. Notably, the U.K. MetOffice (metoffice) has recently implemented a similar WW3-based wave forecasting system. This presents a valuable synergy, in light of ongoing collaborations with the metoffice in relation to NWP.

There are a number of disadvantages associated with the replacement of AUSWAM, as is typical of the upgrading of any mature system, WW3, as tested here, does not include a Data Assimilation (DA) scheme. Considerable effort was put into the assimilation of altimeter data into AUSWAM (e.g. Greenslade, 2001; Greenslade and Young, 2005a; Durrant et al. 2009b), making this loss of capability a major disadvantage. While wave models do not represent an initial value problem, and data assimilation is not critical in order to produce a good wave forecast, it can improve short term forecasts (12 to 24h) in general, and potentially can improve swell prediction for the Pacific Ocean much further into the forecast period. The large impact of DA seen in AUSWAM, however, is due in part to the relatively poor performance of the underlying model. The advantages of DA would be expected to be less with the increased quality WW3. This effort is also not lost, and future work will include the incorporation of DA in the new system.

There are also some potential concerns with the use of WW3 guidance within the current forecasting environment at the Bureau. NWP plays a central role in the forecasting process. Modern forecasting involves subjectively assessing model data and combining this with observations of current conditions and forecaster knowledge to provide local forecasts. These are traditionally produced by individually assessing each site, and manually producing written forecasts for each site. The Graphical Forecast Editor (GFE), developed at NCEP, aims to reduce the load on the forecaster, by allowing NWP gridded data to be graphically manipulated, allowing the forecasters' interpretations of weaknesses in the model guidance to be incorporated (see Glahn and Ruth, 2003). From these manipulated fields, site forecasts can then be automatically produced using computer generated text.

The Bureau has recently implemented the GFE into its operational forecast process (e.g. Treloar 2009; Leeuwenburg 2009). WW3 data will provide the marine forecast input into the GFE. For consistent gridded fields such as H_s and T_p, the transition from AUSWAM to WW3 is transparent from this perspective. However, for fields of partitioned data, the new approach of WW3, though physically more meaningful, is likely to cause some issues for the GFE. These are discussed further in Appendix C.

[2]http://www.nopp.org/funded-projects/fy2009-projects-funded-under-nopp/topic-1-improving-wind-wave-predictions-global-to-regional-scales/

On balance, the case for WW3 is a strong one. However, its performance must be proven to be superior to AUSWAM in order to warrant implementation. The remainder of this report discusses the set up and testing of the model. Comparisons of the accuracy of the wave models themselves are complicated by the parallel replacement of the atmospheric model and the change in the error characteristics of the surface winds associated with this. This is briefly discussed in the following section.

2.3 Forcing Winds

Wave model accuracy depends critically on the accuracy of the surface winds. A 10% error in the estimate of surface wind speed can lead to 10-20% errors in H_s and 20-50% errors in wave energy (Cavaleri, 1994). While the quality of surface winds from NWP systems has increased greatly over the last 10-15 years (e.g. Janssen et al. 2002), there will inevitably remain systematic biases in these fields that contribute to errors in the modelled wave field. As such, a knowledge of the error characteristics of the forcing winds is critical to the interpretation of wave model error.

Previous work has shown that GASP under-predicted surface wind speeds by 5-10% (Kepert et al. 2005; Schulz et al. 2007). The wave model is sensitive to these biases, and had been shown to respond positively to statistical adjustments to remove them (Greenslade et al. 2005).

The Bureau has recently replaced GASP with the ACCESS system, for which the error characteristics of the surface winds are less well known. To address this, a direct assessment of ACCESS global domain (ACCESS-G) marine surface winds has been carried out by Durrant and Greenslade (submitted, hereafter DG11) against QuikSCAT scatterometer data for a period of 4 months from July to October 2008. Overall, it was found that ACCESS-G provides a significant improvement over GASP, with Scatter Index (SI) indicating approximately a 20% improvement in 10m wind speed (U_{10}) at short lead times. Gains in overall forecast skill were found to persist through the forecast period with ACCESS-G providing about a 12h gain in skill over GASP at 24h lead time, increasing to about 24h at 96h lead time.

A low bias was identified in both sets of surface winds, with U_{10} underestimated by approximately 8% for ACCESS-G, and 3% for GASP. The bias was found to be greater in the meridional direction than the zonal. Although the overall bias for GASP was small, significant regional biases were found to exist, with low biases in the mid-latitudes being offset by positive biases in the tropics. ACCESS-G shows more consistency in bias over the globe. These results emphasize the importance of examining the spatial structure of model error, especially in the context of downstream systems.

A knowledge of these error characteristics provides important context for the interpretation of wave model error, with regional biases present in the winds likely to cause corresponding biases in the waves. For the purposes of comparing the error characteristics of the new wave model set-up against AUSWAM, a knowledge of how their respective forcing winds compare also adds greatly to the ability to interpret their differences. As such, appropriate findings from DG11 are referred to in the current wave model evaluation where applicable. The interested reader is referred to the original paper for added detail on the error characteristics of the forcing winds.

3. DATA AND METHOD

This section describes the basic set up of the WW3 model and the testing carried out. Section 3.1 describes how the WW3 model was set up, the model options used, and a description of those options to be tested. Section 3.2 describes the methods used for verifications of the wave model output against both buoy and altimeter data.

3.1 Model Set Up

The WW3 code is modular and is operated by switches chosen at compile time that allow the user to choose specific model options. The input and dissipation source terms for example, are one such package. The following describes how the model was set up, which switches were chosen, the grid and nesting arrangements and input data sets used to construct them.

A number of grid domains and resolutions were tested during the initial model set up, including two way nested grids. In a traditional one way nesting arrangement, in an operational forecast environment, each model grid is run after corresponding wind forcing is available from the atmospheric model. Under a two way mosaic set up (as described in Section 2.2), all the wave model grids are run in parallel, so the entire run must wait until all the winds are available. Hence, due to the sequential way NWP is run, mosaic grids were found to be unsuitable for operational implementation.

The initial ACCESS implementation has been designed to replicate the grid arrangements of the previous GASP system. Wave model grid arrangements are largely constrained by the available forcing winds. Hence, initial grids for the operational AUSWAVE are identical to those used for AUSWAM. These consist of a global grid at 1° resolution, a regional grid at 0.5° resolution and an Australian grid at 0.125° resolution, shown in Fig. 3.1. The wave spectrum is resolved into 24 azimuthal direction bins and 25 frequency bins logarithmically spaced from 0.04118 to 0.4461 Hz. Directional bins are also rotated by half a bin to avoid excessive propagation of energy along the grid axes (Bidlot, 1997), a problem that was previously identified and addressed in AUSWAM (Greenslade, 2000).

The construction of these grids requires bathymetric data. AUSWAM previously used a combination of a bathymetric data set produced by the Australian Geological Survey Organisation in the Australian region, and ETOPO5 elsewhere (Greenslade, 2000). The availability of new data sets in recent years, and the increased importance of accurate bathymetry in the context of the improved shallow water physics of WW3 necessitate a re-evaluation of the best bathymetry for the Australian region.

The data sets examined were:

1. ETOPO2, produced by National Geophysical Data Center (NGDC, 2006).
2. DBDB2v3, produced by the National Research Labs (NRL, 2006). This data set incorporates the Australian Bathymetry and Topography Grid produced by Geoscience Australia (Petkovic and Buchanan, 2002, hereafter GA2002).
3. BLUElink global bathymetry, the data set used by the operational ocean model at the Bureau. This is essentially DBDBv2 using GA2002 in the Australian Region.
4. The Smith and Sandwell global data set, a high resolution bathymetric data set derived by combining available depth soundings with high-resolution marine gravity information from the Geosat and ERS-1 satellites (Smith and Sandwell, 1997).

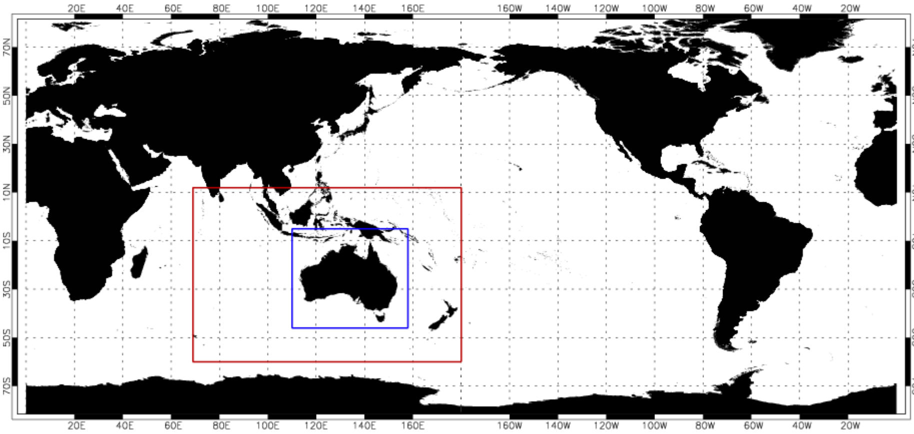

Fig. 3.1 Operational grids for AUSWAVE. Resolutions are 1° for the global grid, 0.5° for the regional grid (red) and 0.125° for the Australian grid (blue).

Wind waves of typical wave lengths only begin to interact significantly with the bottom at depths of 50 m. Hence, it is the accuracy of the data in Australian coastal regions that is of primary interest. To gauge this, comparisons are made with known buoy depths along the Australian coast. The complete list of buoys used can be found in Appendix A. Validations shown in Fig. 3.2 are calculated from buoys in water depths less than 50 m only. Note that ETOPO2 was found to perform very poorly in the Australian region, and is omitted here.

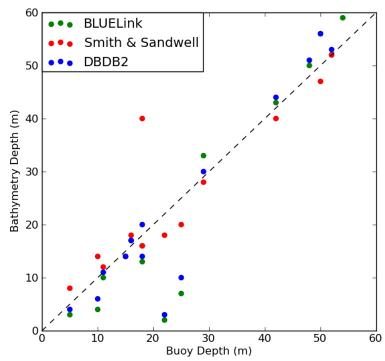

Bath.	Bias	SI	RMSE
BLUELink	-3.92	0.34	8.25
S&S	3.25	0.41	9.35
DBDB2	-2.92	0.31	7.30

Fig. 3.2 Validations of bathymetry data sets at known buoy depths around the Australian coast.

These simple validations suggest that DBDB2v3 is the best data set in the Australian region, though it is difficult to draw definitive conclusions based on these relatively few points of comparison. The DBDB2v3 data set also has the advantage that it extends to 90°N and 90°S, while the BLUElink data only covers up to 76°, allowing more flexibility in the grid choices. The bathymetry for the Australian grid derived from DBDB2v3 is shown in Fig. 3.3.

As discussed in Section 2, WW3 has the ability to account for blocking occurring due to islands that are too small to be resolved explicitly. This requires the input of obstruction grids, indicating the percentage of each grid cell that is blocked in both the x and y directions. The construction of these grids has previously been a manually intensive task. Recently, an algorithm has been developed at NCEP to construct these grids automatically (Chawla and Tolman, 2008). The algorithm accounts for islands overlapping grid cells as well as the orientation of islands in neighbouring cells. In addition to a bathymetry data set, the Global Self-consistent Hierarchical High-resolution Shoreline (GSHHS) coastline dataset (Wessel and Smith, 1996) is used, which resolves small islands and structures that are beyond the capability of the bathymetry. The GSHHS data set, for example, contains 180,509 coastal boundaries, 99%

of which have areas less than 6 km^2. By comparison, the 2’ global bathymetry used here has a resolution of ~14 km^2. Further details about how the obstruction grids are constructed can be found in (Chawla and Tolman, 2008), while technical details on the use of the code can be found in (Chawla and Tolman, 2007).

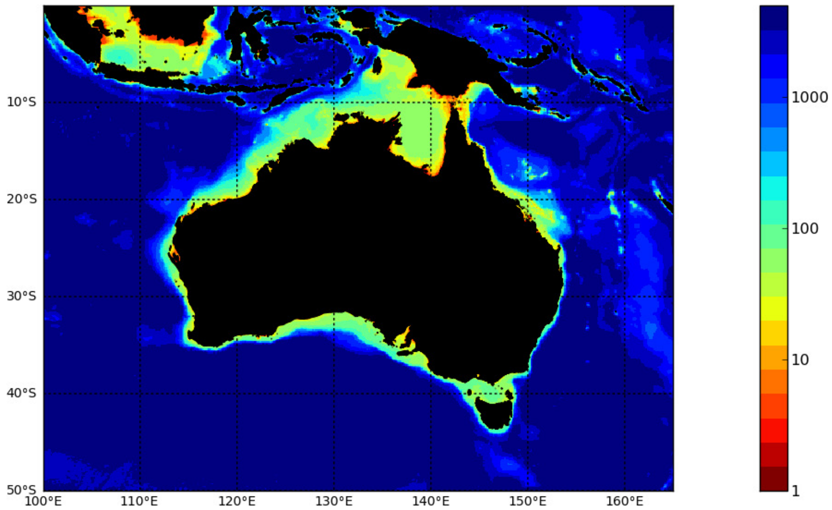

Fig. 3.3 Bathymetry (m) derived from DBDB2 version 3.0 for the Australian grid on a logarithmic depth scale.

Each grid requires four different time steps. The ‘global’ time step, by which the entire solution is propagated in time, the spatial propagation time step, the intra-spectral propagation and the minimum source term integration time step. The minimum source term integration time step refers to the fact that the actual time step within the model is dynamically adjusted as described previously. Time steps and geographical extents for each grid are given in Table 3.1. The time steps have been determined based on efficiency and numerical stability considerations. The fact that the global time step is larger for the regional grid than the global grid is due to the southerly extent of the latter, and the decreasing physical size of grid cells with increasing latitude. Details of how these time steps are determined is described in Appendix B of the WW3 User Manual (Tolman, 2009). The maximum forecast ranges for each grid are dictated by those of their respective ACCESS forcings.

Table 3.1 Details of operational grids. Time steps shown are the global, spatial propagation, the intra-spectral propagation and minimum source term integration respectively.

Grid	Forcing	Domain	Resolution	Lead Time	Time Steps
Global	ACCESS-G	78S - 78N 0 - 360	1°	120 hours	3000, 1000, 1500, 15
Regional	ACCESS-R	60S - 12N 69E - 180	0.5°	48 hours	3600, 1000, 1800, 15
Australian	ACCESS-A	50S - 0 100E - 165E	0.125°	48 hours	1200, 400, 600, 15

Sea ice is accounted for directly using the continuous method of (Tolman, 2003), by which temporally varying obstruction grids are calculated based on local sea ice concentration. Daily

SSMI high resolution sea ice concentration data[3] is ingested for this purpose, retrieved from the Bureau's MARS archive. For hindcast runs, ice is updated daily, for forecast runs, the ice is kept constant at day one concentrations throughout the forecast period

At the time of testing, only the global ACCESS winds were available, and during early testing, all grids were run using the global winds. For this reason, the focus of this report is on the global results only. All WW3 test runs are forced with winds from test ACCESS-G runs from the 00ho experiment run by NMOC. This experiment is very close to the system that was implemented operationally in August 2010. Based on the availability of these winds, a four month period was examined, from 1 July 2008 to 1 November 2008. This represents a highly active period of wave generation in the Southern Ocean, providing a good test period for the model in the Australian region. However, further testing of the model on a seasonal basis is warranted to examine performance in a range of generating conditions, such as monsoonal winds and the shifting of the Southern Ocean storm belts. This is left here for further work.

A number of hindcasts were performed here to assess, in a broad sense, the most suitable choices for the initial configuration of the model for the Australian region. The focus here is on the choice of source terms, but the impact of propagation numerics and sub-grid-scale blocking are also considered. Default parameterisations are used for all source term options. A list of runs performed is presented in Table 3.2, and described further in the following text. Each run was initialised using JONSWAP spectra and spun up for the full month of June.

3.2 Method

Verifications were carried out against both buoy and altimeter observations. The following section describes these data, and the procedure used to verify the model.

Table 3.2 Hindcasts performed.

Name	**Source Terms**	**Blocking**	**Numerics**
TC96	*Tolman and Chalikov* (1996)	Yes	UQ
WAM3	*Komen et al.* (1984)	Yes	UQ
BAJ	*Bidlot et al.* (2007)	Yes	UQ
BAJ-1st	*Bidlot et al.* (2007)	Yes	1st order
BAJ-NoSub	*Bidlot et al.* (2007)	No	UQ

3.2.1 Buoy Verifications

Buoy verifications are carried out at a number of buoy locations around the Australian coastline. The global model examined here, at 1° resolution, would not be expected to produce realistic values in around complex coastlines. Hence, only buoys located in water deeper than 40 m are used here. Additionally, in locations where the nearest model grid point was significantly offshore from the buoy location, the buoy was not used. The locations of the buoys used for verification of the model runs in this work are shown in Fig. 3.4. For the purposes of reporting here, statistics are divided into groups of buoys as indicated in Fig. 3.4. These groups are based on geographical location, and the type of waves likely to be encountered in each region. Buoys 56004, 56005 and 56006 have been grouped with 55040 and 55026 for example, as these regions all encounter waves coming directly off the strong winds and long fetches of the Southern Ocean. Statistics are calculated and reported separately for each of these buoy groups.

[3]http://polar.ncep.noaa.gov/seaice/hires/global.xml

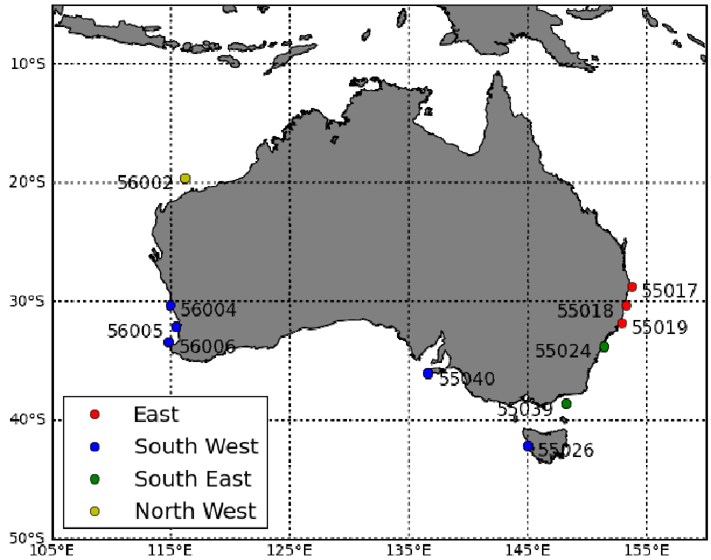

Fig. 3.4 Australian buoys used in this study. Buoy groups mentioned in the verifications statistics are indicated.

Some simple quality control checks are carried out on the buoy data prior to use: non-physical values are removed, a check for faulty instruments removes more than four consecutive observations of the same value, and a check for consistency with neighbouring observations is performed. The data is generally of high quality, and the quality control required is minimal. An example is shown in Fig. 3.5 for the Crowdy Head buoy (55019) for the month of July 2008.

Observations of H_s are available from some of the buoys at half-hourly intervals (55040 and 55026), some of the buoys at hourly intervals (55018, 55019, and 55022) and the remainder at 3-hourly intervals. The 3-hourly model time series is linearly interpolated to the observation times. In the spatial domain, if the four surrounding model grid points are sea points, the model is bi-linear interpolated to the buoy location, if one of these points is a land point, the nearest model grid point used.

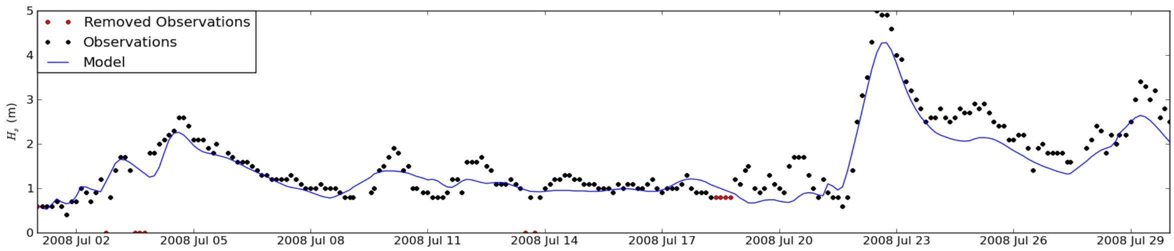

Fig. 3.5 Crowdy Head (55019) H_S buoy data for the month of July 2008, with observations removed by automatic quality control shown in red.

These buoys provide a very important method of model validation. Their position on the Australian coast, and the fact that they provide continuous time series make them a valuable source for evaluating the model in the regions where it is largely utilised, i.e. around the Australian coast. In addition to H_s, buoys also provide a means of verifying model T_p.

However, due to the fact that they are located on or near coastlines, in areas that are inherently hard to model due to local coastal effects such as shallow water and island blocking, they must be used with some caution, and they cannot be considered to represent the overall error characteristics of the model in the open ocean. Hence, buoy verifications should, where possible, be supplemented with altimeter verifications.

3.2.2 Altimeter Verifications

Radar altimeters are active microwave sensors which infer H_s directly from the shape of the radar pulse, or waveform, returning to the nadir-looking altimeter. The two altimeters used here are the Poseiden-2 altimeter onboard Jason-1 (Menard et al. 2003; Carayon et al. 2003) and the RA-2 altimeter of Envisat (Resti et al. 1999). Jason-1 has a prograde orbit of 66°, while Envisat has a retrograde orbit of 98°, allowing measurement closer to the poles. The combination of these two altimeters provides good spatial coverage of the worlds' oceans, and offers an invaluable source of data for operational wave modelling, both for data assimilation and verification. Typical observations during a 24 h period for both altimeters are shown in Fig. 3.6.

Altimeter data are of high quality, with error variances being comparable to those of in-situ buoy data (Caires and Sterl, 2003). They do however, typically contain systematic biases (e.g. Cotton and Carter, 1994) that must be removed. Following Durrant et al. (2009a), a small linear correction is applied to Envisat prior to use:

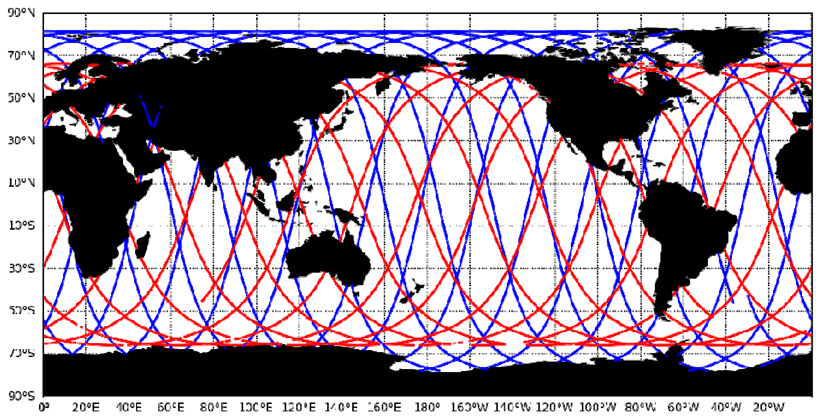

Fig. 3.6 Altimeter ground tracks from one day for Jason-1 (red) and Envisat (blue).

$$H_s^{corrected} = 1.041 H_s^{observed} - 0.076 \tag{3.1}$$

The same authors found no corrections were necessary for Jason-1.

Altimeter data is also known to contain erroneous observations that must be removed. Prior to assimilation in AUSWAM, the method of Young and Vledder (1993) was used, consisting of an initial check for gross error against the first guess model field, followed by a cross validation check for consistency with other nearby data. This serves to remove erroneous data, with the comparison with the first guess field also limiting shocks to the model. For the purpose of validation however, quality control should be done independently of the model. A check is performed based on the standard deviation of the 20Hz and 10Hz H_s values for Jason-1 and Envisat respectively (Mackay et al. 2008), and nearest neighbour comparisons are performed to remove any remaining obvious errors. In order to match the spatial scales of variability between model and observations, 'super-obs' are then calculated by performing 1° along track averages, consisting of 15-20 individual observations (e.g. Tolman et al. 2002; Janssen, 2008). This is demonstrated in Fig. 3.7.

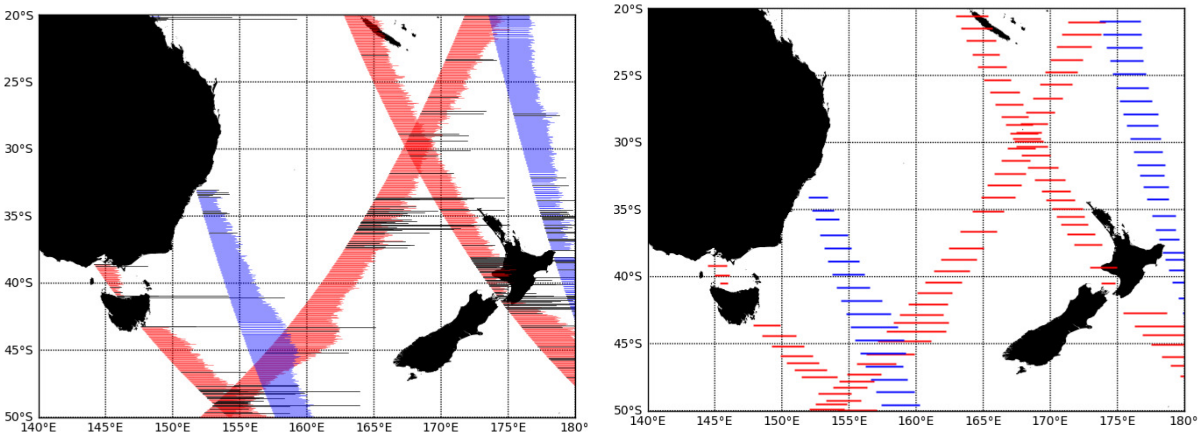

(a) (b)

Fig. 3.7 Jason-1 (red) and Envisat (blue) data over the Tasman Sea for 10th July 2008. (a) shows all data with those removed through the quality control checks shown in black, and (b) super-obs calculated from the remaining data.

In general, wave model verification relies on the interpolation of the model data to the observation location to obtain a set of co-locations. Here, model data is interpolated to match the time and location of the altimeter observation by a cubic spline method to make up a set of co-locations, from which statistics can be calculated. Over the July - November 2008, period examined here, this analysis resulted in more than 580,000 co-locations. Calculating statistics based on these co-locations gives an overall description of the error.

To determine the spatial variation in error, the co-locations are additionally binned into 3° x 3° latitude-longitude bins, and statistics are calculated for each bin separately. When choosing an appropriate latitude/longitude box size, a balance must be struck between resolution and the robustness of the resulting statistics for each box due to increased number of observations. A value of 3° was found to be a good compromise. It is also worth noting that the physical size of a 3° box reduces at higher latitudes. However, due to the orbital characteristics of the satellite, the density of the observations also increases at higher latitudes, maintaining sufficient observations in these smaller boxes.

The total number of co-locations in each box over the 4 month period is shown in Fig. 3.8. There are reduced numbers of co-locations along coastlines and around islands for obvious reasons. Sea ice around Antarctica results in no co-locations around this continent, with the shifting ice edge over this period resulting in a gradual reduction in the number of co-locations around the edge. The maximum seen between 60° and 65° N is due to the orbital characteristics of the altimeters. Over most of the globe, there are around 150 co-locations for each 3° x 3° bin.

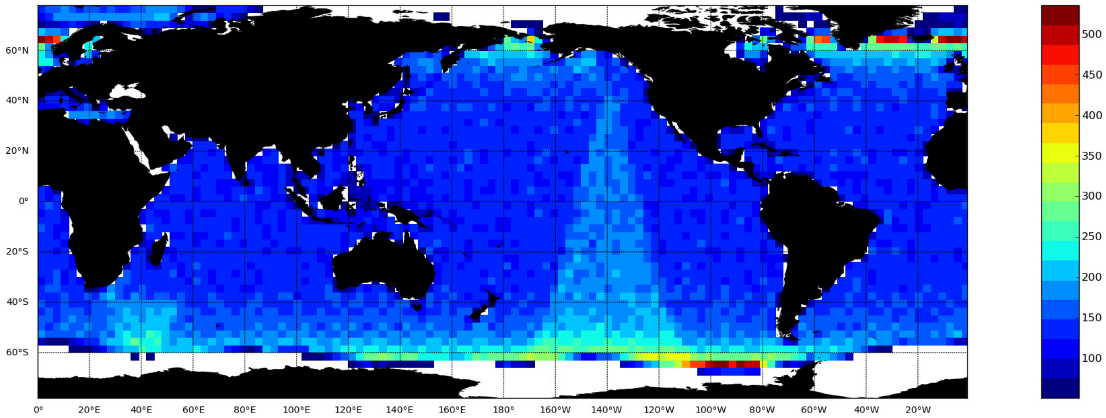

Fig. 3.8 Number of co-locations.

Statistics referred to throughout this report are the bias, the slope of the regression line through the origin, the RMSE, the SI (standard deviation, divided by the mean observed value) and the correlation coefficient (*R*). Definitions of these statistics are as follows:

$$Bias = \frac{1}{N}\sum_{i=1}^{N} M_i - O_i \tag{3.2}$$

$$RMSE = \sqrt{\frac{1}{N}\sum_{i=1}^{N}(M_i - O_i)^2} \tag{3.3}$$

$$SI = \frac{\sqrt{\frac{1}{N}\sum_{i=1}^{N}\left(\left(M_i - \overline{M}\right) - \left(O_i - \overline{O}\right)\right)^2}}{\overline{O}} \tag{3.4}$$

$$R = \frac{\sum_{i=1}^{N}\left(M_i - \overline{M}\right)\left(O_i - \overline{O}\right)}{\sqrt{\sum_{i=1}^{N}\left(M_i - \overline{M}\right)^2\left(O_i - \overline{O}\right)^2}} \tag{3.5}$$

$$slope = \frac{\sum_{i=1}^{N} O_i M_i}{\sum_{i=1}^{N} O_i^2} \tag{3.6}$$

where M_i is the model, O_i is the observation, N is the number of co-locations and an overbar represents the mean value.

Each of these measures has strengths and weaknesses. We focus on the bias and the SI which gives an indication of typical scatter around this bias. It is worth noting, that in areas of persistently low wave heights, the SI can give high values, even though the RMSE associated with these errors is small. Similarly, in such areas, small absolute biases, can be associated with large relative biases (as indicated by the slope). In instances where presenting all these statistics is impractical, relevant commentary is made in the text.

4. RESULTS

Results are presented here in two parts. In Section 4.1, various model options are tested in order to come up with a WW3 configuration suitable for operational implementation. This configuration is then compared to the previous operational model in Section 4.2.

4.1 AUSWAVE Configuration

The focus here is on the choice of source term options that give the best results in the Australian region. Additionally, the impact of the numerical scheme is discussed in Section 4.1.2, and the broadscale effect of sub-grid-scale blocking is presented in Section 4.1.3. All hindcast runs are performed over the same 4 month period (July - October 2008). The focus here is on wave model performance, hence high quality short term forecast winds (0-12h) are used, longer range forecasts will be examined in the context of AUSWAVE comparisons in Section 4.2.

4.1.1 Physics

The original WAM3 source terms were based on Snyder et al. (1981) and Komen et al. (1984). As mentioned previously, AUSWAM uses a slightly modified version of these WAM3 terms. During the development of these source terms, testing was performed for wind sea growth in the absence of swell, which was later found to have unnatural effects on the corresponding model results (Tolman and Chalikov, 1996). This problem is inherent to the definition of a mean steepness based on the entire spectrum and leads to over-estimations of wind sea growth in the presence of swell (e.g. Cavaleri et al. 2007). The release of WAM4 1991 included updates to these source terms based on Janssen (1991). This change resulted in an increased growth rate for young wind sea over that of older wind sea (Bender, 1996). Further changes to the dissipation formulations used by ECMWF gave more emphasis on the high-frequency part of the wave spectrum resulting in a more realistic interaction between wind sea and swell (Bidlot et al. 2007).

The original release of WW3 employed the source term package of Tolman and Chalikov (1996, hereafter TC96) consisting of the input source term of Chalikov and Belevich (1993) and Chalikov (1995) and two dissipation constituents. These claimed to provide improved results on global scales when compared to WAM3 terms (e.g. Tolman et al. 2002).

WW3 has retained the option to use WAM3 source terms within the WW3 model framework. In the most recent release (version 3.14), WAM4 source terms have also been added (Ardhuin et al. 2007), matching the formulations of Bidlot et al. (2007, hereafter BAJ).

This section presents an analysis of model runs performed using these three source term packages (see Table 3.2). Spatial results over the whole globe are presented to give a context to the error characteristics associated with each, followed by an analysis against buoy data around the Australian coast. As the development of both TC96 and BAJ terms were motivated by the desire to correct known deficiencies in the WAM3 terms, they can be expected to produce improved results. WAM3 terms are included here, partly for completeness, but also as they provide a useful comparison to the AUSWAM system, which uses slightly modified versions of these terms (Bender, 1996).

The total wave model error is of course the result of error in the wave model itself, as well as due to imperfect forcing winds. The translation of error in the forcing winds into the wave model is not straightforward. Locally, wind errors will produce errors in newly generated wind sea. These errors will also present as errors in the swell propagating away from the generation region. Hence, the wave error at any given point associated with incorrect wind forcing is a result of the integration of wind error over a window of time and space. The addition of error due to an imperfect wave model make the attribution of error a non-trivial exercise. However, by comparing the error characteristics of several source term packages when using the same forcing, some general observations can be made.

Historically, the comparison of TC96 and WAM source term variants has been hampered by the fact that they could only be used within WW3 and WAM respectively, introducing the added complication of having to account for additional differences in the models themselves (such as numerics, sub-grid-scale blocking, shallow water effects etc.). The ability to run all these source term packages from within the same model removes this complication.

The aim is to determine, in a fairly broad sense, which source terms are the most suitable in the Australian region. A factor in this choice is the degree to which a given source term package "matches" the ACCESS forcing winds. Though the focus here is not the attribution of forcing/wave model error, knowledge of the error characteristics of the wind provides a much needed context to the discussion. As such, the ACCESS evaluation carried out by DG11 will be referred to where appropriate.

A summary of the H_s verification statistics for the three source term packages are shown in Fig. 4.1 for both buoys and altimeters. Focusing initially on the altimeter results, all three show negative bias, with WAM3 showing the most by a significant margin, and TC96 showing the least. Overall, the RMSE is comparable for both BAJ and TC96, with the negative bias in both being slightly greater for BAJ, and the SI of BAJ being marginally better than that of TC96. It is argued here that this common negative bias is largely, if not wholly, the result of a significant negative bias in the forcing winds identified by DG11, discussed in Section 2.3.

Examining these error statistics in a spatial context, Fig. 4.2 shows bias and SI over the globe for each of these source terms. Though clear differences exist, the low bias in H_s is present for all source term options over much of the globe. Similar spatial error plots for the forcing winds relative to QuikSCAT scatterometer data can be found in DG11. Though a detailed analysis of how these spatial wind errors manifest in the wave field is not presented here, it is clear that given the low bias in the winds over much of the globe, a low bias in the waves is not a surprising result. It is in this context that the comparison of source terms below is made.

WAM3 shows a more severe low bias than both BAJ and TC96. This low bias in the WAM3 formulations has been noted by several other studies (e.g. Lionello et al. 1992; Bender and Glowacki, 1996; Rogers, 2002). BAJ and TC96 also produce much better results than WAM3 in terms of SI over the whole globe. Given the clear superiority of these terms, in the context of choosing the best option for the operational system, the following discussion focuses only on these two source term packages.

There are notable features common to both BAJ and TC96 error characteristics. Both show high SI to the north of Indonesia. These are primarily due to low wave heights in this region. Absolute values in terms of RMSE are less severe (not shown). The low bias in this region is of note in the context of the wave climate, with slope indicating strong underestimations (not shown here). Though the models (both atmospheric and wave) can be expected to show relatively large variable error in these areas of low wind speed and wave height, data quality is also likely a contributor, with increased relative scatter expected.

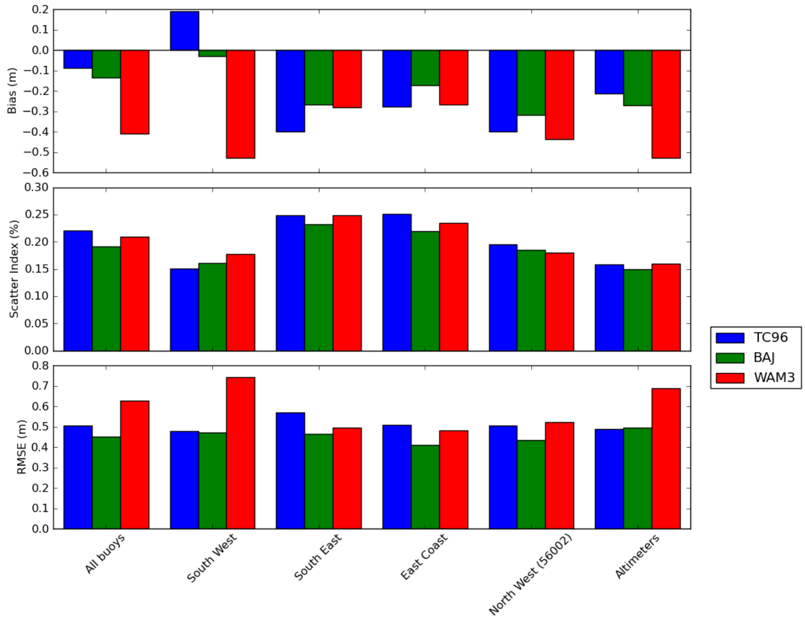

Figure 4.1 Overall H_s statistics for BAJ, WAM3 and TC96 source term packages relative to buoy and altimeter data.

High SI can be seen around coastlines. There are a number of factors likely contributing to this error such as, errors associated with poorly resolved coastal processes within the wave model, ocean surface current systems and error associated with the inaccurate wind forcing. At this resolution, little can be concluded about the relative role of shallow water effects. It is apparent that in the south of the African, South American and Australian continents, bias and SI are worse on the east coasts. This is consistent with wind error being the major cause of error in these predominantly young, fetch limited wave conditions. Indeed, a low bias in the wind speed was identified at the coast by DG11, which is likely producing biases as well as variable error that is imparted onto the wave field. While this suggests that wind error is the major cause of error here, further scrutiny would be required to assess this quantitatively.

Despite these similarities, clear differences can be seen in the error characteristics between these source terms. Noting here the time of the year, most of the swell in the tropical regions is coming from the storm tracks in the Southern Ocean. TC96 shows a positive bias to the south of Australia which extends into the south and Tropical Eastern Pacific. A stronger local positive bias is produced by the BAJ terms in the Tropical Eastern Pacific, despite a negative bias in the generation areas of the southern mid-latitudes. This is due primarily to a lack of swell dissipation in WAM variant source terms (including BAJ). Observations of swell dissipation are consistent with the effect of friction at the air-sea interface, resulting in a flux of momentum from the wave field to the wind (Collard et al. 2008). This flux is entirely absent from WAM source term variants, while TC96 includes swell attenuation by the wind, based on numerical simulations of the airflow above waves (Chalikov and Belevich, 1993). Notably smaller SI in the Tropical Pacific for TC96 than for BAJ can likely be attributed to the inclusion of this effect in the former. The contribution of swell dissipation to the overall wave spectral balance has been added to the WAM source terms in the recent formulations of Ardhuin et al. (2010), but these are not tested here.

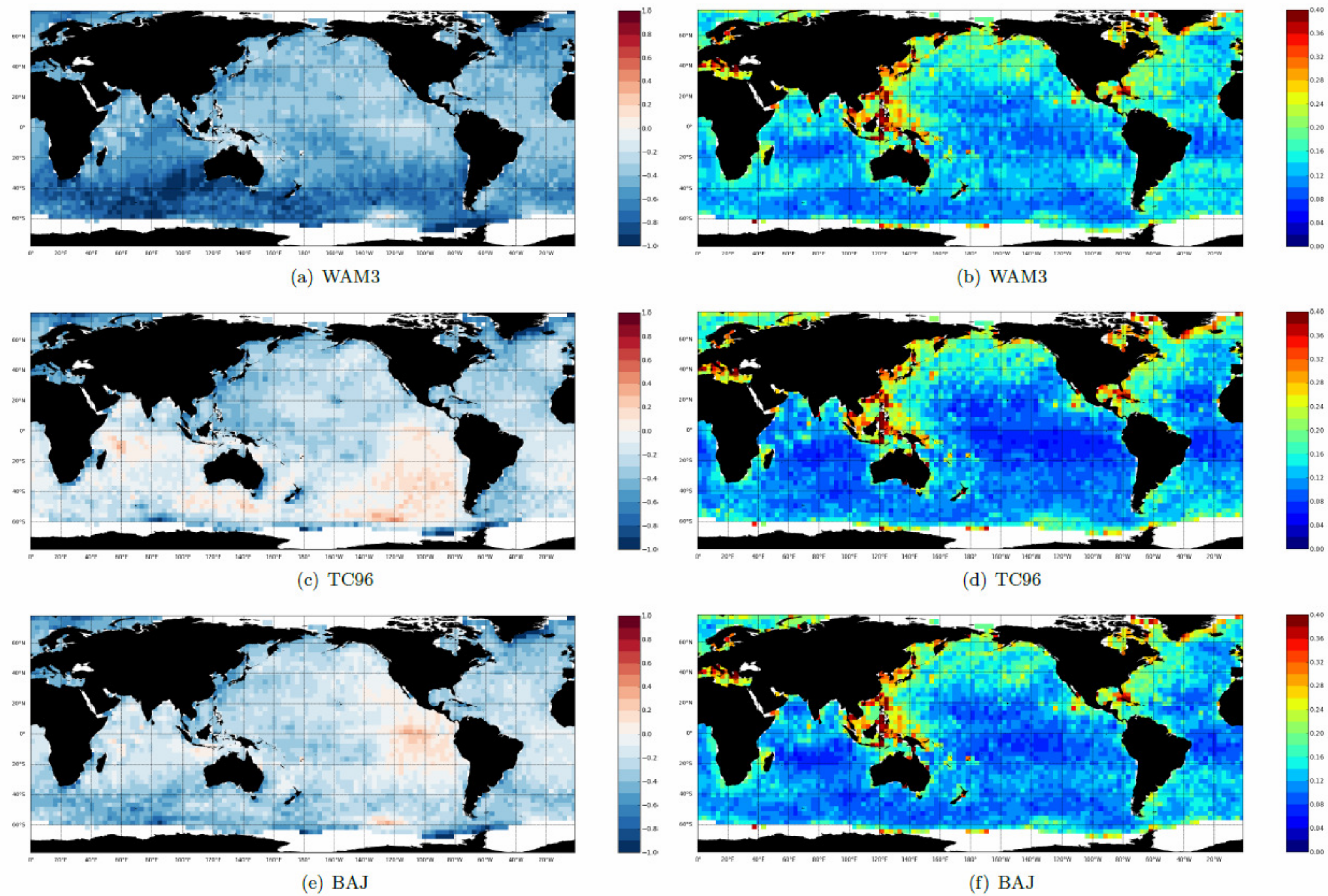

Figure 4.2 Spatial plots of H_s bias (left hand column) and SI (right hand column) for TC96, BAJ and WAM3 source terms calculated against Jason-1 and Envisat data.

The positive bias present for TC96 in the Southern mid-latitudes is notable due to the fact that the winds are known to be biased low in this region. This suggests that with unbiased winds, TC96 would produce waves that are too energetic in these generation areas of the Southern Ocean. This is supported by ongoing operational verifications performed at the Bureau. The Bureau currently receives operational wave forecasts from both the NOAA and the United Kingdom Met Office (UKMO) wave models. Both of these systems are based on recent versions of WW3, both using TC96 source terms. Ongoing monthly verifications of both wind and waves from these models (Bidlot et al. 2002[4]), show that both of these centres have winds that do not show the degree of negative bias that ACCESS does. From operational buoy verifications, and through anecdotal evidence from forecasters, these models consistently show a significant positive bias on the Australian west coast.

This is consistent with the findings of Rogers (2002) who has shown from growth curves that WAM (in this case WAM4) is more energetic than WW3 for short fetches, while WW3 is more energetic for long fetches. This is perhaps indicative of the fact that tuning for TC96 was done with an emphasis on accuracy in the Northern Hemisphere, having not been tuned to handle the long fetches present in the southern ocean. BAJ also shows better SI than TC96 in these regions.

This is also evident in the buoy verification (Fig. 4.1). In general, these buoy results give similar conclusions to the altimeter data, indicating even more strongly that BAJ outperforms TC96 in regions around the Australian coast. For SI, BAJ outperforms TC96 at all regions except the South West. For bias, while TC96 shows the lowest bias when averaged across all regions, BAJ shows more consistency across buoy locations. The magnitude of the bias for each region is smaller for BAJ, and is negative everywhere, while TC96 produces a positive bias for the South West buoys and a negative bias at all other locations. This is consistent with TC96 inherently over predicting in the long Southern Ocean fetches within a general state of negative bias due to the forcing winds.

T_p verifications are also shown in Fig. 4.3 (note that there are no T_p statistics for altimeter data). Overall, WAM3 shows a clear negative bias. TC96 shows a slight negative bias with BAJ indicating negligible biases. In terms of SI, results are comparable for TC96 and BAJ, both showing gains over WAM3. Overall, it is difficult to draw any definitive conclusions in regards to T_p.

To summarise, BAJ has been found to produce the best results in the Australian region. Though the overall bias is reduced for TC96, evidence suggests that TC96 is actually biased too high, especially in the Southern Ocean, and this is being mitigated by a low bias in the ACCESS winds. It could be argued that it is favourable to choose a source term package that will compensate for known deficiencies in the wind. However, as the wind biases can be expected to improve with time, the pursuit of the most accurate wave forecast under unbiased winds must be the end goal.

[4]http://www.jcomm.info/index.php? option=com_content&task=view&id=107

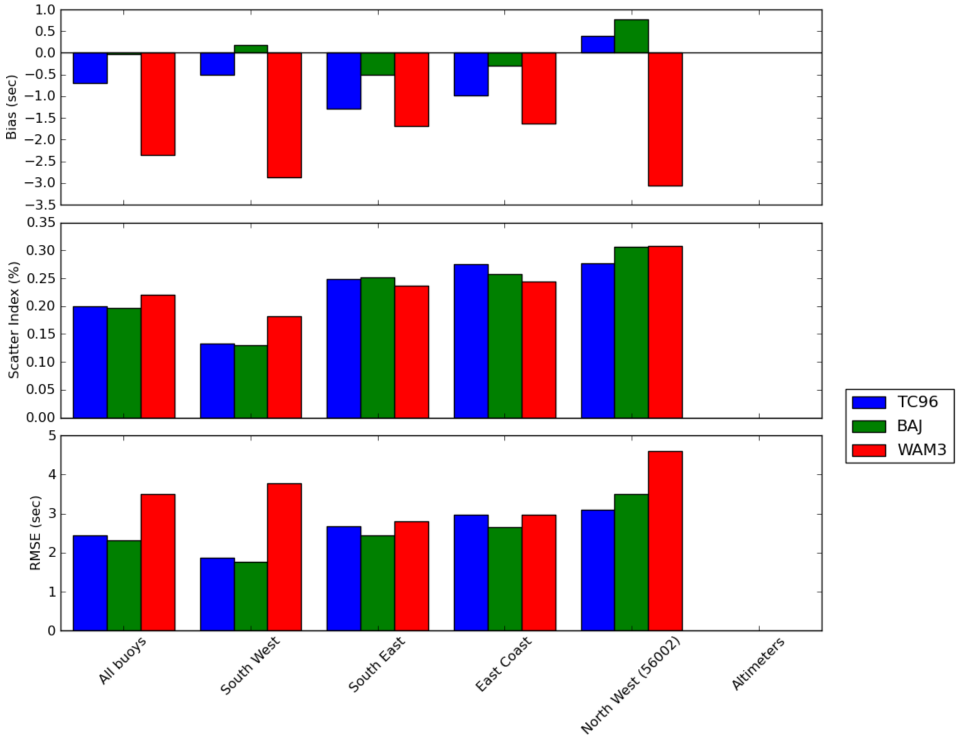

Figure 4.3 Bias and SI for different source term options.

4.1.2 Numerics

Both WAM and WW3 include, or have been used with, higher order schemes which can be employed as an alternative to the explicit, first order upwind scheme. The higher order scheme used in WAM is the second order leapfrog scheme (which has zero numerical diffusion). The higher order scheme of WW3 is the UQ scheme and limiter (Tolman, 2003; Leonard, 1979, 1991). This scheme is third order accurate in both time and space.

The default numerical scheme in WW3 is the UQ scheme, though the model also includes a first order scheme. The third order scheme is generally considered superior, with the latter being included mainly for testing purposes. However, despite the obvious attraction of higher order schemes, there remains some contention as to their benefit in the context of wave modelling.

The most recent implementation of AUSWAM used the third order upwinding scheme of *Bender* (1996). From verifications of a one month hindcast using three buoys located around the Australian coast, it was concluded that the first order upwinding propagation numerics of WAM were responsible for excessive dissipation of wave energy, particularly swell, causing negative biases in H_s on much of the Australian coastline. This has since been refuted by Wittmann and O'Reilly (1998) and Rogers (2002) who have subsequently shown with the use of a great circle ray tracing tool, that the first order numerical scheme of WAM is unlikely to be a primary source of negative bias in the model operated at FNMOC. Furthermore, Rogers (2005) make the point that all the numerical schemes used in these models are mass conserving, so while they be may indirectly responsible for local biases in conjunction with island blocking for example, overall, they do not dissipate energy, and cannot be responsible for biases.

Though it is easily demonstrated that a first order scheme can not adequately advect a spike of energy, in real world wave modelling applications, the structure of the wave field is rarely this extreme. It has been suggested that, at least in the case of integrated parameters, there is little to be gained from these higher order schemes (Rogers et al. 2005; Cavaleri and Bertotti, 2006).

Figure 4.4 shows time series of both H_s and T_p for both numerical schemes at the Cape du Couedic waverider buoy. Some smoothing is visible, though it does not appear to be a large effect. However, this time series is dominated by wind sea, smoothing is likely to be more significant for swell systems.

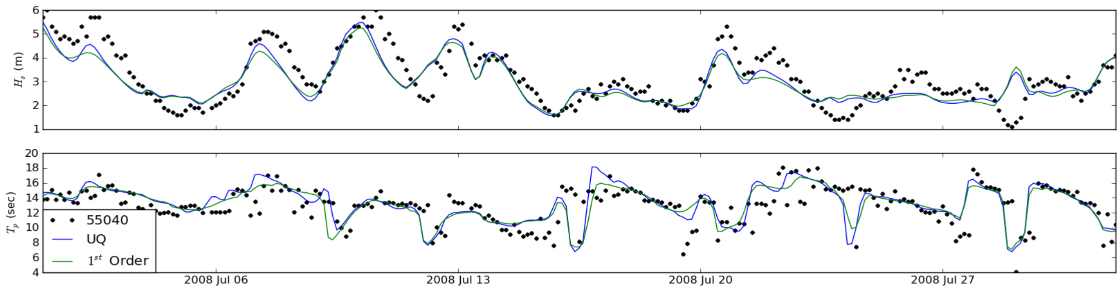

Figure 4.4 Time series of (a) H_s and (b) T_p for both the UQ and 1st order numerical schemes at the Cape du Couedic waverider buoy for the month of July 2008.

To examine the influence of numerics, model runs using both the first order and the UQ scheme were performed. Runs are otherwise identical, both employing BAJ source terms. Statistics for these runs based on buoy and altimeter verifications are shown in Fig. 4.5. These show an increased negative bias in the UQ results, contrary to the assertions of Bender (1996). Differences are more pronounced for buoy results, showing consistent differences across all regions. In terms of SI, though differences are small, again they are more pronounced in the buoy data, suggesting that the choice of numerical scheme is having a bigger impact at the coast than in the open ocean.

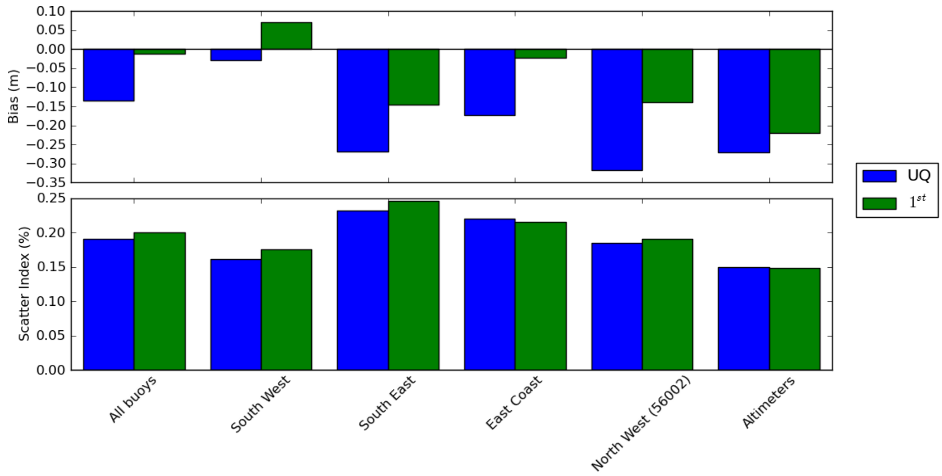

Figure 4.5 Statistics for 1st order and UQ numerical schemes relative to buoy and altimeter data.

This can be clearly seen by examining the difference between the model H_s means for each scheme, shown in Figure 4.6. Locally differing bias characteristics are visible in the lee of islands. The origins of these differences are not entirely clear. Both schemes are expected to produce unrealistically smooth shadow zones in island wakes, though for different reasons. In the case of the first order scheme, this is due to lateral numerical diffusion. For the UQ numerics, Tolman (1995) demonstrates that the use of the Booij and Holthuijsen (1987) diffusive GSE correction in the UQ produces the same defect. Similar results are shown for the averaging GSE alleviation, used here, by Tolman (2002b). Quantitative differences in the severity of this deficiency may locally account for some of these differences. (Note that an alternative method is proposed by Tolman (2002b), in which divergence is added to the advection field, with this technique noted by the author as potentially allowing for GSE alleviation without removing shadow zones behind islands. However, this is not included in the current version of WW3 due to a lack of maturity).

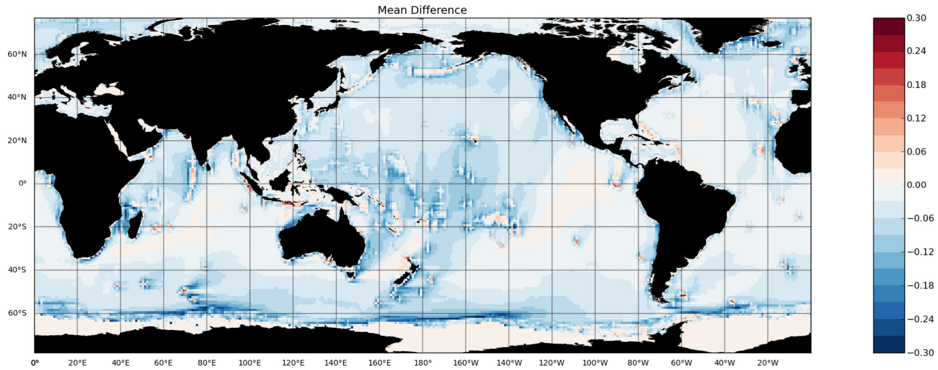

Figure 4.6 Mean difference (m) between H_s from the 1st order and UQ numerical schemes (UQ – 1st).

In their ray tracing experiments, Rogers (2002) examined a number of swell systems travelling from the southern Pacific at buoy locations off the Californian coast. Due to a lack of land interference in this scenario, the island shadowing effect would not have been present. Hence, while their assertion that the choice of numerical scheme does not affect the overall global bias, due to their conservative properties, it is clear from the results presented here, that while this is true of unobstructed wave propagation, the excessive land shadowing effect can produce significant overall biases.

This is an additional source of negative bias off the southern East Australian coast, discussed above. Figure 4.6 shows a significant wave shadow in the wake of Tasmania, adding to wind related bias already present. This is evident in the south east and east coast buoy results (Fig. 4.5).

Despite altimeter verifications indicating similar values of SI for both numerical schemes for the global data set, significant spatial variation is apparent. Figure 4.7 shows the spatial distribution of the percentage improvement in SI for UQ over the first order scheme, with improvements evident over much of the globe, with the exception of the eastern Tropical Pacific. At first glance, this is a surprise given the predominance of swell in this region. However, we have shown that the BAJ source terms result in a lack of attenuation of swell in this region (discussed above), and the UQ scheme is most likely simply correctly propagating these deficiencies.

It is also worth making the point here, that applying point based verifications to a spatial forecast, in this instance gives the 1st order scheme an advantage in terms of these verification statistics. For example, in addition to error in the intensity of a storm, there is also a phase error, or location error. If a storm's intensity is predicted correctly, but it is misplaced in space or time, comparisons with a passing altimeter track will result in a large error both at the location of the model maximum, and where that maximum actually is. A numerical scheme that smoothes out the field, will record a lower error in both locations, so while a correctly placed storm verifies better in the UQ scheme, an incorrectly placed storm verifies better for the more diffusive 1st order scheme. In many applications, a storm whose intensity is correctly forecast but slightly misplaced is more desirable than one whose intensity is under-predicted. This is not necessarily reflected in the verification statistics.

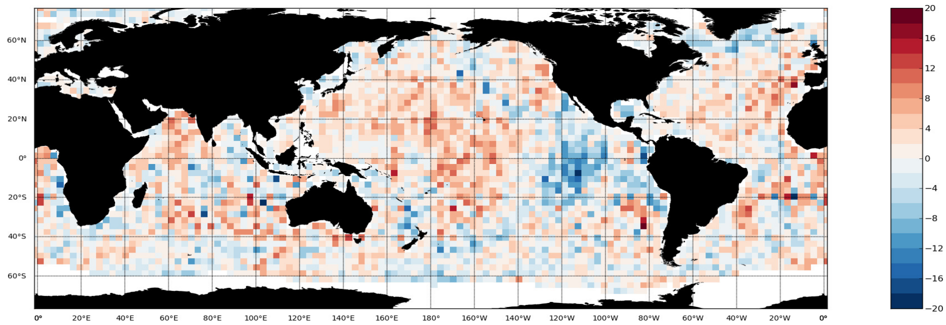

Figure 4.7 Percentage improvement in H_s SI for UQ over the 1st order scheme

Despite inconclusive results for the use of the third order scheme, the authors tend to agree with the conclusions reached by Cavaleri et al. (2007), that is that if methods are available to compute propagation more accurately without a large increase in computation time, then these methods should be used. In this case, it is clear that the variable error improves with the use of higher order numerics. The fact that the first order scheme masks the problem of an existing low bias is not an argument for its use. As stated previously, the best possible forecast under unbiased winds must be the aim, and the superposition of opposing error sources is not a desired outcome. In addition, in the context of an operational forecast model, the ability to accurately predict the extremes is paramount. Hence, the UQ scheme is recommended for use in the operational implementation.

4.1.3 Sub-Grid-Scale Blocking

The following section examines the influence of sub-grid-scale blocking on the large scale error. Comparisons are made between runs performed with and without sub-grid-scale blocking active. These runs use BAJ source terms, and UQ numerics.

For illustrative purposes, an example of the effect of sub-grid-scale blocking on the propagation of a swell field through French Polynesia is shown in Fig. 4.8. In the absence of such blocking, more wave energy is passing through the island chain.

The effect of sub-grid-scale blocking is also evident on the large scale. From the spatial bias and SI plots shown in Fig. 4.9, the impact is not only local, but extends far beyond the location of the obstruction. In this particular case, the effect of unblocked swell incorrectly propagating from the southern ocean generation regions into the Pacific is evident throughout the Tropical Pacific and extending up into the North Pacific.

Though not verified here, the effects of sub-grid-scale blocking on the performance of the model against buoys inside areas such as the Great Barrier Reef can be expected to show significant improvement. This blocking is active in each of the nested grids, resulting in improved boundary conditions supplied to the inner grids due to the blocking of wave energy through French Polynesia for example, as well as an improved representation of blocking by the reef itself within the inner grids. As wind forcing was not available for these inner grids at the time of testing, these verifications are not carried out here. It is suggested that a thorough evaluation of the effects of sub-grid-scale blocking on the modelling of waves in the reef region would be highly valuable.

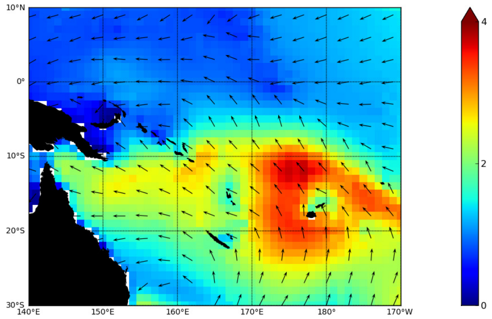

(a) Sub-grid-scale blocking

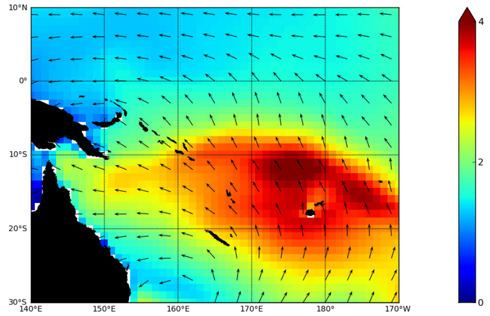

(b) No sub-grid-scale blocking

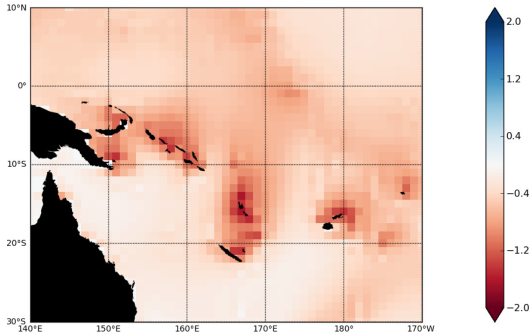

(c) Difference ((b)-(a))

Figure 4.8 H_s (m) for a wave system propagating northward through French Polynesia using BAJ source terms and UQ numerics with (a,c) and without (b,d) sub-grid-scale blocking activated and the difference between the two (c).

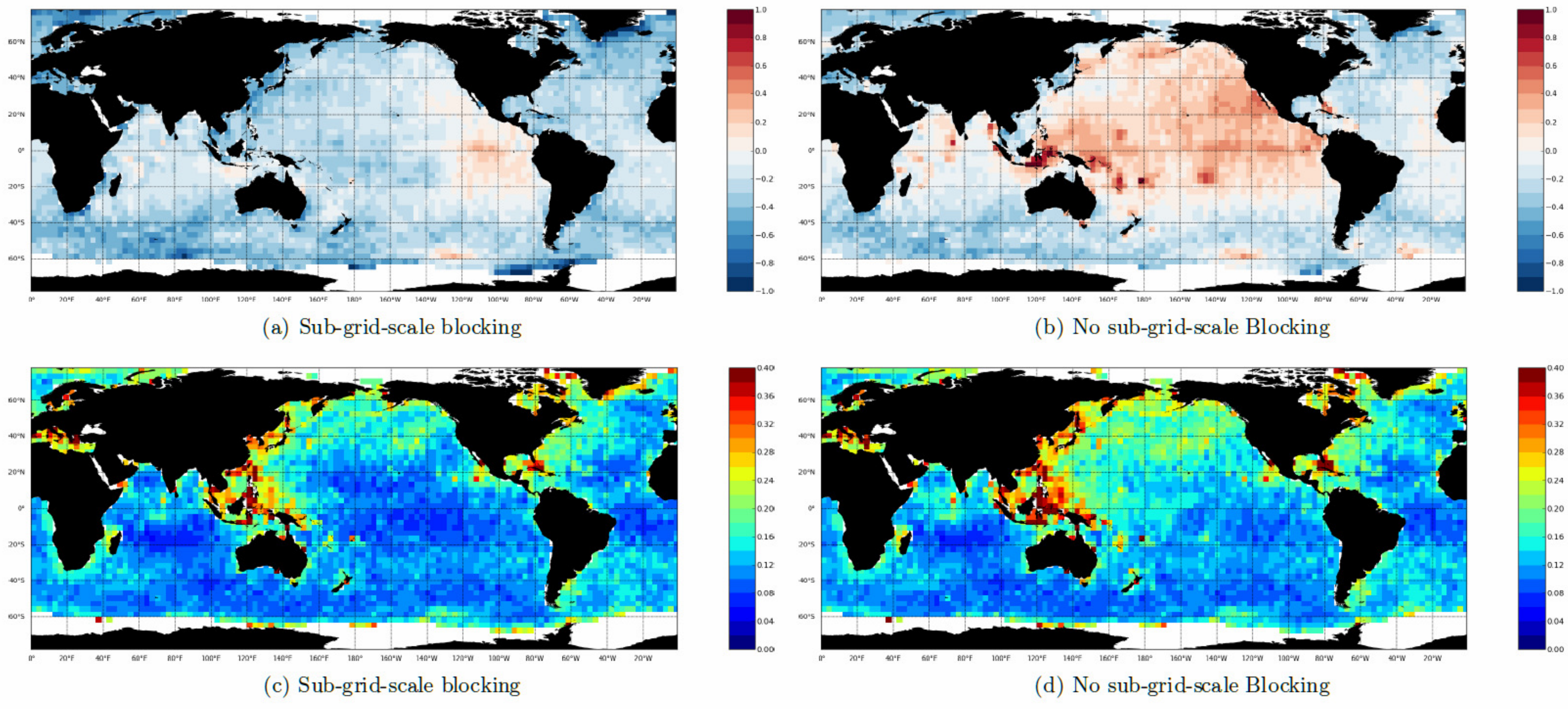

(a) Sub-grid-scale blocking

(b) No sub-grid-scale Blocking

(c) Sub-grid-scale blocking

(d) No sub-grid-scale Blocking

Figure 4.9 Hs spatial bias (m) and SI for BAJ with (a, c) and without (b, d) sub-grid-scale blocking activated. Both runs use UQ numerics.

Based on the results presented above, the configuration chosen for AUSWAVE employs BAJ source terms, using the UQ numerics with sub-grid-scale blocking active. This configuration is compared to AUSWAM output for this same period in the following section.

4.2 Comparison with AUSWAM

The following section discusses how the AUSWAVE model compares to the AUSWAM. This is not an entirely straightforward comparison, as there are some differences that make a model to model comparison difficult. The major obvious difference is the different wind forcing applied to each model. In addition, AUSWAM includes data assimilation, while AUSWAVE does not, meaning that, at least for the analysis, as altimeter data is assimilated, it can not be considered independent here. Also, while the ice edge is partly accounted for in AUSWAM by setting the wind to zero, there are still some large errors around the ice edge due to the absence of wave energy being completely removed when it encounters the ice edge.

Given these difficulties, this section will aim to discuss in general the characteristic errors of AUSWAM, what has been improved in AUSWAVE, and the errors that remain. The focus here is on the end user and what they can expect from the new model implementation.

To gain an overall comparison of AUSWAVE and AUSWAM, Fig. 4.10 shows the error as a function of forecast period against both buoys and altimeters. Error differs significantly for the buoy and altimeter data. This is not unexpected, as the buoy data represents a small area of the Australian coastline, whereas the altimeter data is representative of error over the whole globe. These differences are discussed further below. Some conclusions relating to characteristic differences between the models can, however, be drawn from this plot.

Focusing initially on the bias, it is clear that for short lead times, a positive bias for AUSWAM contrasts with a negative bias for AUSWAVE. However, throughout the forecast period, the AUSWAM bias steadily declines. By about four days lead time, biases are similar. This is due to the data assimilation scheme, which reduces the inherent model biases at the analysis time. Durrant et al. (2009b) noted that innovations during the data assimilation cycle were predominantly positive for AUSWAM. DG11 showed that the negative biases in GASP winds are less prominent than those in ACCESS. This suggests that, contrary to the ACCESS forced AUSWAVE, the bias in the GASP-forced AUSWAM is due primarily to a bias in the wave model itself.

In the case of both models, the bias is more negative when compared to altimeter data than buoy data. This difference on its own is not overly surprising, as they are based on different geographical areas, with different wave climates. However, the possibility remains that the model is not accurately capturing the processes in the coastal regions where the buoys are located, especially considering the 1° resolution of the model as tested here. It is also interesting to note that while the ratio of the difference between the buoy and altimeter bias remains fairly constant through the forecast period in the case of AUSWAVE, it converges in the case of AUSWAM. This is due to changing spatial characteristics of the errors with forecast period, and some cancellation of positive and negative bias over the whole globe from the altimeter comparisons. This is discussed in more detail below.

For the SI, AUSWAVE shows significant improvement over AUSWAM. At short lead time, the benefit of the DA is apparent for AUSWAM, though these gains are quickly lost. Despite the fact that altimeter data has been assimilated into AUSWAM, AUSWAVE shows improved variable error even at the analysis. Overall, AUSWAVE produces a consistent 36 to 48 hour gain in model forecast skill over AUSWAM.

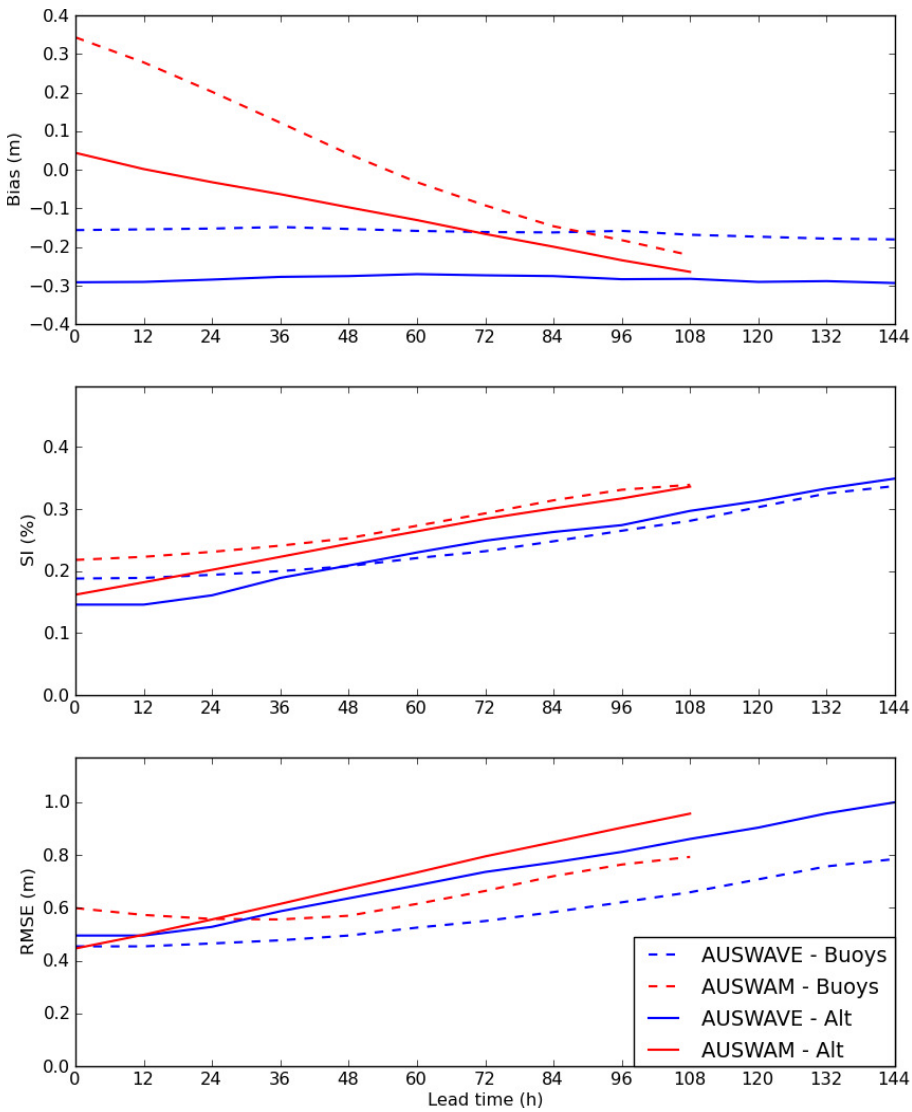

Figure 4.10 Error as a function of forecast period.

Figure 4.11 shows spatial plots of bias and SI from comparisons with altimeter data for 12 - 24h lead time. For AUSWAVE, the bias pattern has previously been discussed in section 4.1.1, and reflects the bias in the surface winds. For AUSWAM, we can see that the bias is negative in the mid latitudes, and positive in the tropics. This spatial pattern resembles that of the GASP forcing (DG11), though it is likely that additional error is being introduced by the wave model. In the mid-latitudes, for example, biases are comparable to those of AUSWAVE, despite less severe negative biases in the winds. From the previous discussion, this is likely the result of the WAM3 source terms. Similarly, it is clear from the positive bias in the lee of major island chains, that a neglect of island blocking is also contributing to the positive bias in the tropics.

As forecast period increases, and the effects of the data assimilation in AUSWAM fade, this pattern becomes more pronounced. Figure 4.12 shows similar plots for 84 - 96h lead time. The pattern of negative bias in the mid latitude storm tracks and positive bias in the Tropics has become more pronounced for AUSWAM, while for AUSWAVE, the bias pattern remains similar. AUSWAVE is showing lower SI than AUSWAM everywhere except in the far Northern latitudes.

This spatial pattern in the AUSWAM bias can explain the relative differences between the altimeter and buoy's bias growth with forecast period seen in Fig. 4.10. While the majority of buoys are in the mid-latitudes, and thus see the effects of the rapidly increasing negative bias there, for the altimeters, the globally averaged bias decreases at a reduced rate due to a relative constant bias in the tropics. This again highlights the value of examining these spatial plots when considering altimeter data, and the added insite that can be gained over examining buoys in isolation.

For the SI, AUSWAVE shows clear improvement over AUSWAM at both of these lead times. SI is significantly lower in all major ocean basins. This can be more clearly seen in Fig. 4.13 indicating percentage improvement in SI of AUSWAVE over AUSWAM. The greatest gains can be seen around the ice edge and in the Tropics. The positive impact of the inclusion of sea ice and sub-grid-scale blocking are evident, with these areas indicating improvements above 50%. Significant gains are evident over most of the globe.

Buoy verifications of H_s (Fig. 4.14) show similar improvements to those of the altimeter verifications. The relative low bias of the AUSWAVE system is apparent for all buoys. It is particularly pronounced for the South East coast buoys. As discussed previously, this is likely the contribution of negative biases in the ACCESS winds in this region. The differing spatial evolution of error discussed above is consistent with these results. For example, for AUSWAM, the increasing mid-latitude bias is evident in the south west buoy results while this trend is less severe in the north west. The AUSWAVE forecast exhibits more consistency with regard to buoy locations. Time series of H_s at each buoy location for AUSWAVE and AUSWAM are presented in Appendix B.

For T_p, shown in Fig. 4.15, gains are even greater. This is not a surprise, due to expected gains from the BAJ source terms, as well as a lack of data assimilation, which is known to have detrimental effects on T_p forecasts (Greenslade and Young, 2005b).

The spatial error plots presented above provide useful insight into model error characteristics. These become even more informative when combined with similar analysis of the error in the forcing winds. However, when examining multiple models, at several lead times with different forcing, it is useful to present this information in a more condensed form. One useful way to do this is with the use of Taylor diagrams (Taylor, 2001). These diagrams provide a concise statistical summary of how well patterns match each other in terms of their correlation, their root-mean-square difference, and the ratio of their variances. Statistics can also be normalised, allowing more than one variable to appear on a single diagram. This feature makes them a useful tool for visualising error in both the wave field and the forcing wind field.

Taylor diagrams for both AUSWAM and AUSWAVE are presented in Fig. 4.16. In order for the geometry of the diagram to work, centred RMSE must be used, i.e. that calculated after the mean of both the model and the observations have been subtracted (Note that this quantity, referred to as centred RMS by Taylor (2001) is essentially the standard deviation of the difference between model and observations):

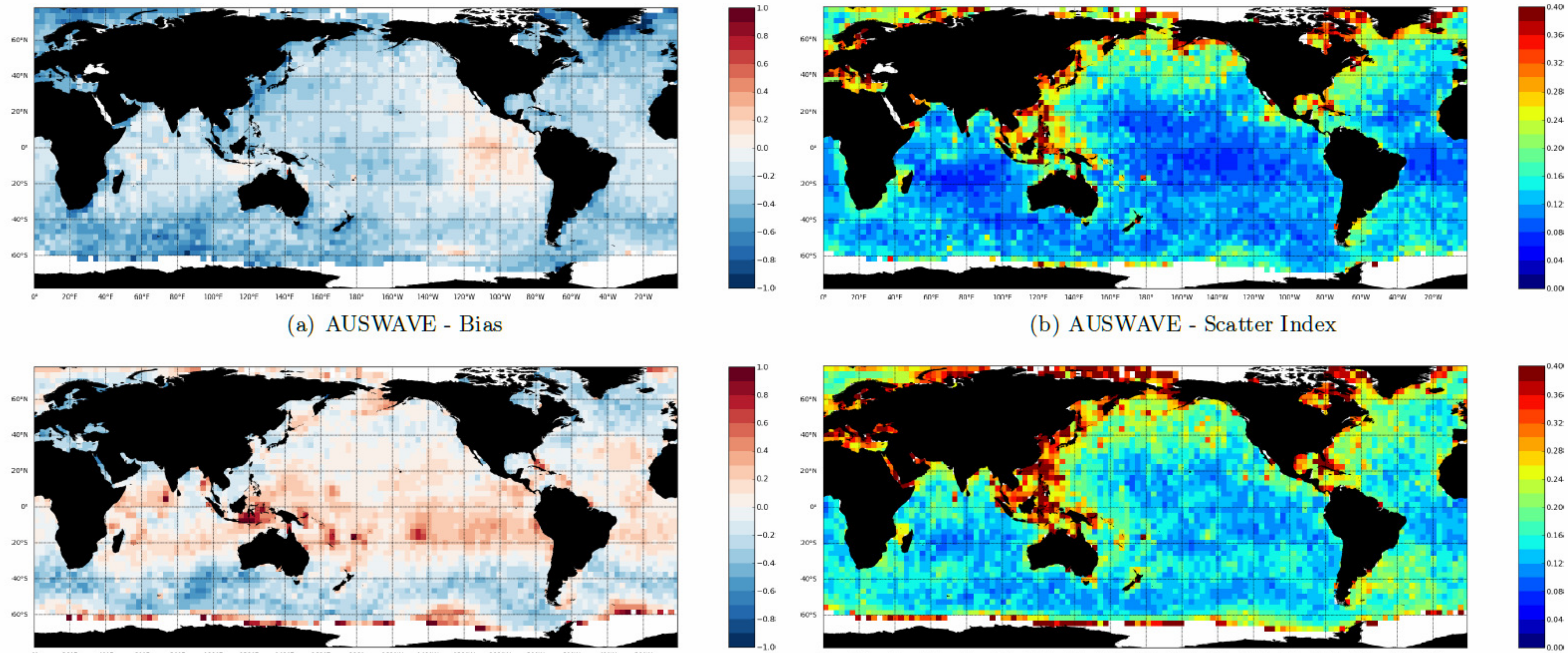

(a) AUSWAVE - Bias

(b) AUSWAVE - Scatter Index

(c) AUSWAM - Bias

(d) AUSWAM - Scatter Index

Figure 4.11 Bias and SI for AUSWAM and AUSWAVE for 12-24h Hs forecasts.

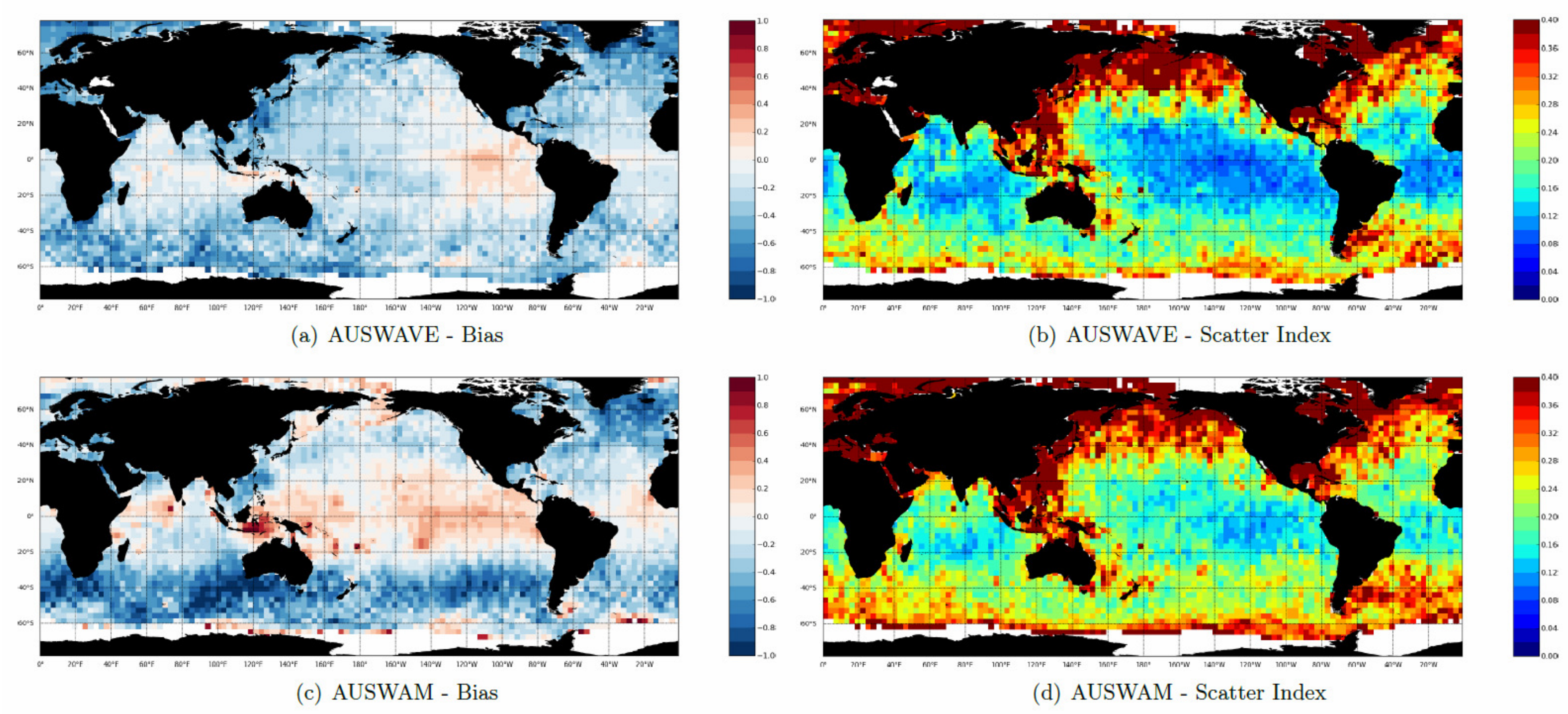

Figure 4.12 As for Figure 4.11 but for 84-96h forecasts

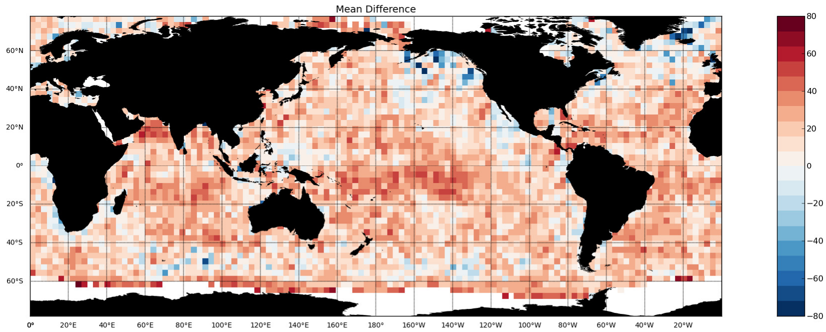

Figure 4.13 Percentage improvement in SI for AUSWAVE over AUSWAM for 12-24 hour H_s forecast.

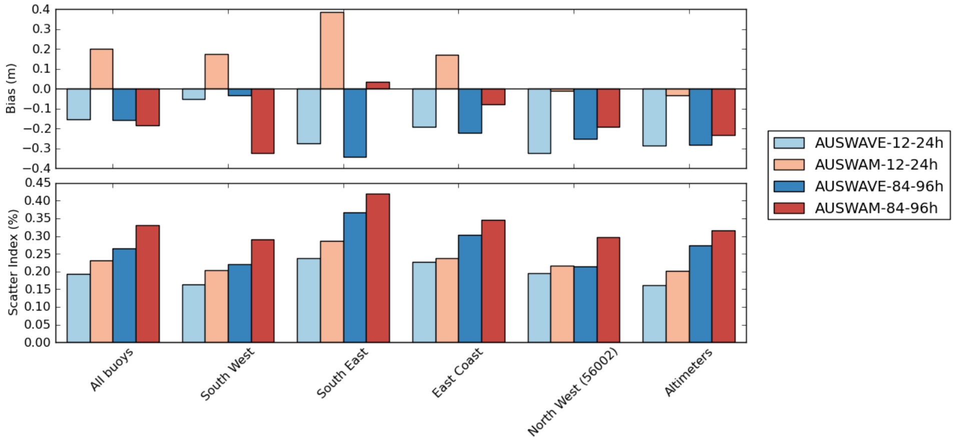

Figure 4.14 Bias and SI for analysis, 24h and 96h H_s forecasts against buoy data.

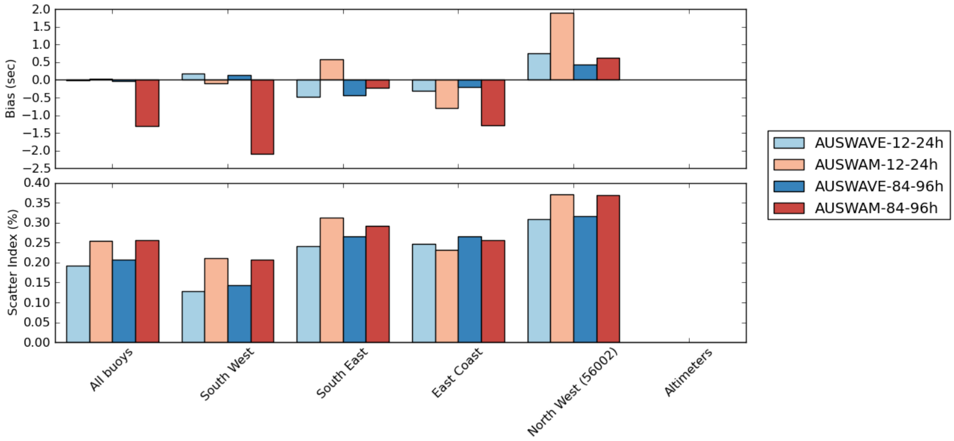

Figure 4.15 Bias and SI for analysis, 24h and 96h T_p forecasts against buoy data.

$$RMSE_{centred} = \left\{ \frac{1}{N} \sum_{i=1}^{N} \left(\left(M_i - \overline{M} \right) - \left(O_i - \overline{O} \right) \right)^2 \right\}^{\frac{1}{2}} \tag{4.1}$$

As such in, this form, they do not contain information about biases. This is indicated here by the colours of the dots. Note that each variable has a separate colour bar. The centred RMSE and model standard deviation, σ_{mod}, have been normalized by the observation standard deviation σ_{obs}. This allows multiple parameters to be plotted on the same diagram. In this case, both H_s and U_{10} have been plotted. U_{10} statistics have been calculated from QuikSCAT scatterometer observations, as in DG11, and H_s statistics are relative to altimeter observations.

The σ_{obs} is indicated with a dashed line (by definition 1 here in this normalised form). A model whose σ_{mod} is less than that of the observations, will appear on the origin side of this line, while one that contains too much variation will appear on the outer side of this line.

Examining these plots, many of the features discussed previously can be seen. For GASP and AUSWAM, overall bias in the wind and waves increases with forecast period while bias remains almost steady for AUSWAVE and ACCESS. As you would expect, RMSE increases and corr decreases with forecast period.

These plots effectively highlight some of the gains made by the new system. Examining the winds first, while RMSE has been reduced at each forecast period, the variational error shows that ACCESS winds are a little damped relative to GASP. For the waves, despite the better sd of the GASP winds, the waves appear highly damped. The DA improves this, but as lead time increases, the variance of the wave field decreases. The new system appears far better in this regard. The variational error in the waves is still a little damped, but matches that seen in the winds.

Clear gains have been made here in both the waves and the surface winds. In terms of SI, DG11 demonstrated forecast skill of 12h to 24h lead time for the winds. This improved forcing, combined with the clear advantages of AUSWAVE over AUSWAM have been shown here to produce gains of 36h to 48h in SI for the waves. While both models exhibit a negative bias in the Southern Ocean, the source of this bias is not the same. In the case of AUSWAM, though partly due to a negative bias in the winds, is likely due primarily to the use of WAM3 source terms. For AUSWAVE, the majority of the bias appears to be a result of a low bias in the ACCESS winds.

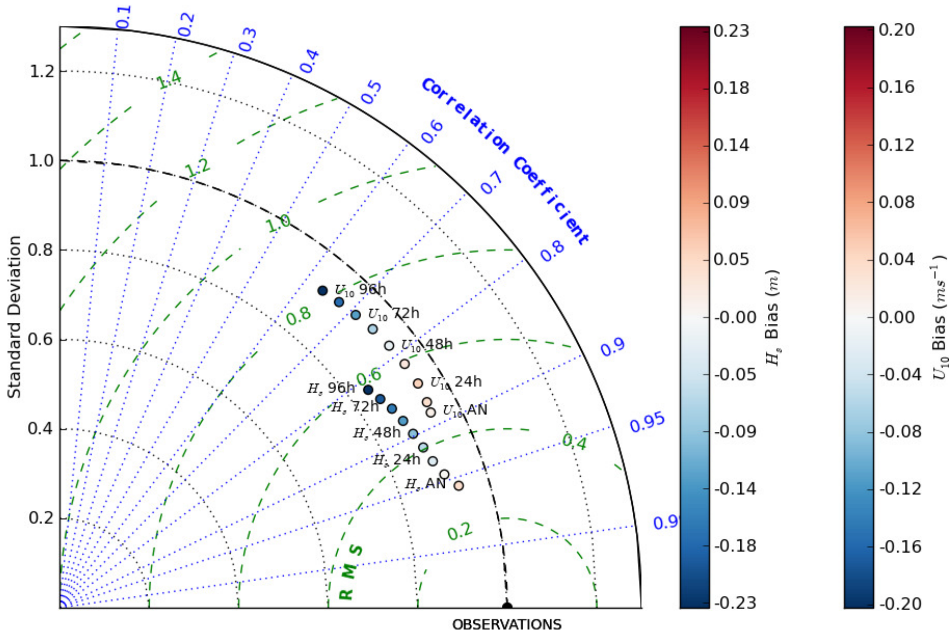

(a) AUSWAM under GASP winds

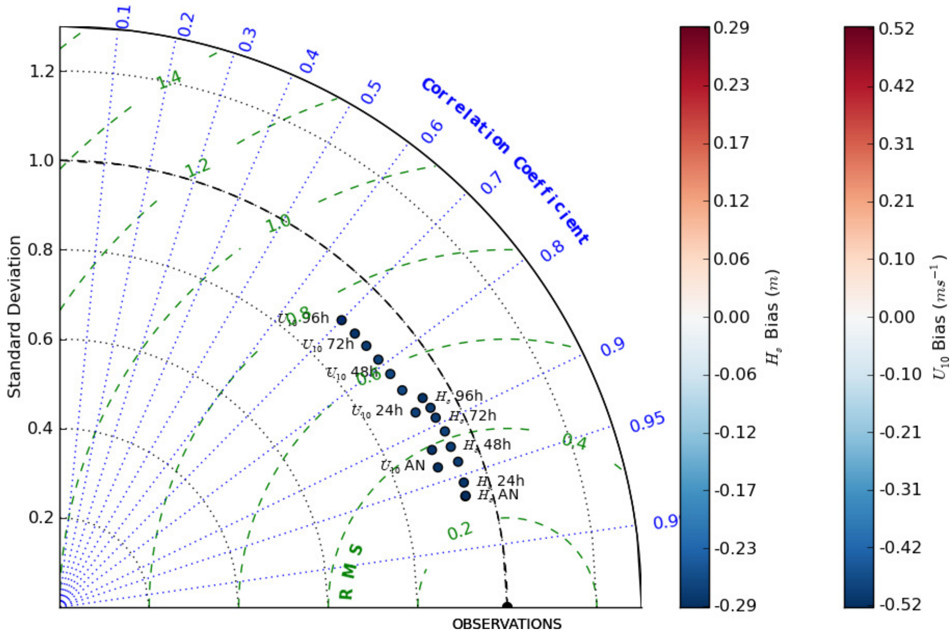

(b) AUSWAVE under ACCESS winds

Figure 4.16 Taylor diagrams of H_s and U_{10} for (a) GASP-AUSWAM and (b) ACCESS-AUSWAVE. Only every second forecast period has been labelled here for clarity. See text for details.

5. SUMMARY AND CONCLUSIONS

5.1 Conclusions

This report has documents the set up and verification of the Bureau's new WW3 based operational wave model AUSWAVE. Evaluation of a number of hindcasts has been carried out to determine a suitable configuration for the operational system. Performing hindcast verifications on WAM3, TC96 and BAJ source term formulations has led to the conclusion that the latter are the most suitable for the Australian region, as they provided the best results when compared against both buoy and altimeter data.

A low bias is present in all WW3 based hindcasts. This is attributed mainly to a known low bias in the ACCESS forcing winds. In this context, TC96 was found to over-predict in the long fetches of the Southern Ocean, resulting in over-predicted H_s values on the west coast. The UQ numerical scheme was found to produce better SI values than the 1st order numerical scheme. However, it was noted that these numerics produced increased wave blocking in the lee of islands. This effect in the lee of Tasmania tended to increase this negative bias on the Australian east coast.

The error characteristics of the ACCESS-driven AUSWAVE have been compared to the GASP-driven AUSWAM system. AUSWAVE has been found to provide clear and immediate improvements over the AUSWAM model, with SI showing forecast skill gains of 36 h to 48 h lead time for H_s. Examining spatial error characteristics of H_s in the context of known characteristics of the wind error has proven to be a useful analysis tool for model diagnostics, with the negative bias in H_s in AUSWAVE largely attributable to a low bias in the ACCESS surface winds. There are several ways to address this bias, including potentially tuning the model source terms, or preprocessing the forcing winds. This will be investigated in further work.

In addition to the improvement in forecast skill demonstrated here, the implementation of the WW3 model also provides opportunities to both benefit from and contribute to the growing international community of WW3 users and developers.

5.2 Further work

The verifications presented here are by no means exhaustive. The aim of this work was to determine a suitable model set up, and evaluate the merits of model options such as numerics and source terms. This initial implementation was deliberately designed to replicate much of the set-up of AUSWAM. As is always the case with a new system, there are avenues open for improvement on the initial configuration.

Further evaluation of the nested grids in the operational system is required to assess the skill of the new model in shallow water regions. It is suggested that a thorough evaluation of the effects of sub-grid-scale blocking on the modelling of waves in the reef region would be highly valuable.

WW3 has the ability to partially incorporate the effects of atmospheric stability in the calculation of surface stress (Abdalla and Bidlot, 2002). Current development of coupled ocean/atmosphere models at the Bureau will likely allow for the incorporation of these capabilities in the near future. The incorporation of ocean surface currents from OceanMAPS could also be explored.

The under-attenuation of swell in the Eastern Pacific has been identified as an issue with the BAJ source terms employed here. Amongst other improvements, this has been addressed in the recent source term formulations *of Ardhuin et al. (2008*, 2010) through the addition of a swell dissipation term based on observations of swell *decay by Collard et al. (2008*). These new formulations have been shown to reduce the positive bias in the Eastern Pacific, and produce improvements over the BAJ source terms over much of the globe. These formulations warrant testing in the Bureau's operational system.

Though the mosaic grid approach described in Section 2.2 is not currently operationally practical, the use of this feature still provides valuable functionality, and paths for upgrades. The possibility of implementing a high resolution grid that conforms to the Australian coastline is a useful feature of the WW3 model. These possibilities will be explored in future changes to the operational grids.

The possibility of performing corrections to the wind fields prior to forcing the wave model can also be investigated. The consistent bias correction over the whole domain employed by Greenslade et al. (2005) could be extended to a spatially varying correction based on statistics presented by DG11. This could also be extended to incorporate aspects of a learned, automated bias correction scheme such as is employed in the Operational Consensus Forecasting (Woodcock and Engel, 2005) this has been demonstrated to have a positive impact on marine winds for site based data (Durrant et al. 2009c).

5.3 Acknowledgments

The authors would like to thank Hendrik Tolman and Arun Chawla (NCEP) for the provision of the WW3 code prior to its initial release. We would also like to thank Paul Sandery and Mark Hemer for their helpful comments on the manuscript.

6. REFERENCES

Abdalla, S. and Bidlot, J. Wind gustiness and air density effects and other key changes to wave model in CY25R1, *ECMWF Technical Memorandum*, 2002.

Ardhuin, F. and Herbers, T. Bragg scattering of random surface gravity waves by irregular seabed topography, *Journal of Fluid Mechanics*, 2002.

Ardhuin, F., Herbers, T.H.C., van Vledder, G.P., Watts, K.P., Jensen, R. and Graber, H.C. Swell and Slanting-Fetch Effects on Wind Wave Growth, *Journal of Physical Oceanography*, *37*, 908–931, 2007.

Ardhuin, F., Collard, F., Chapron, B., Queffeulou, P., Filipot, J. and Hamon, M. Spectral wave dissipation based on observations: a global validation, in *Proceedings of Chinese-German Joint Symposium on Hydraulics and Ocean Engineering, Darmstadt, Germany*, pp. 391–400, 2008.

Ardhuin, F. et al. Semi-empirical dissipation source functions for ocean waves: Part I, definition, calibration and validation., *Journal of Physical Oceanography*, 2010.

Battjes, J. and Janssen, J. Energy loss and set-up due to breaking of random waves, in *cedb.asce.org*, pp. 569–587, 1978.

Bender, L.C. Modification of the physics and numerics in a third-generation ocean wave model, *Journal of Atmospheric and Oceanic Technology*, *13*, 726–750, 1996.

Bender, L.C. and Glowacki, T. The assimilation of altimeter data into the Australian wave model, *Aust. Met. Mag*, *45*, 41–48, 1996.

Bender, L.C. and Leslie, L.M. *Evaluation of a Third Generation Ocean Wave Model for the Australian Region*, 1994.

Bidlot, J.A. Modified Set Up of the Advection Scheme in the ECMWF Wave Model, *Tech. rep.*, European Centre for Medium-Range Weather Forecasts, 1997.

Bidlot, J.R., Holmes, D.J., Wittmann, P.A., Lalbeharry, R. and Chen, H.S. Intercomparison of the performance of operational ocean wave forecasting systems with buoy data, *Weather and Forecasting*, *17*, 287–310, 2002.

Bidlot, J.R., Janssen, E.M. and Abdalla, S. A revised formulation of ocean wave dissipation and its model impact., *Tech. rep.*, ECMWF, 2007.

Booij, N. and Holthuijsen, L.H. Propagation of ocean waves in discrete spectral wave models, *Journal of computational physics*, *68*, 307–326, 1987.

Brassington, G.B., Warren, G., Smith, N., Schiller, A. and Oke, P.R. BLUElink - Progress on operational ocean prediction for Australia, *Bulletin of the Australian Meteorological and Oceanographic Society*, *18*, 104–109, 2005.

Caires, S. and Sterl, A.Validation of ocean wind and wave data using triple collocation, *Journal of Geophysical Research*, *108*, 3098, 2003.

Carayon, G., Steunou, N., Courri\'ere, J.L. and Thibaut, P. Poseidon-2 Radar Altimeter Design and Results of In-Flight Performances, *Marine Geodesy*, *26*, 159–165, 2003.

Cavaleri, L. Wave models and input wind, in *Wave Dynamics and Modelling of Ocean Waves*, edited by G. J. Komen, S. Hasselmann, M. Donelan, L. Cavaleri, and P. Janssen, pp. 283–284., Cambridge University Press, 1994.

Cavaleri, L. and Bertotti, L. The improvement of modelled wind and wave fields with increasing resolution, *Ocean Engineering*, *33*, 553–565, 2006.

Cavaleri, L., Alves, F., Ardhuin, A., Babanin, M., Banner, K., Belibassakis, M., Benoit, M., Groeneweg, J. and Herbers, T. Wave modelling The state of the art, *Progress In Oceanography*, *75*, 603–674, 2007.

Chalikov, D. The parameterization of the wave boundary layer, *Journal of Physical Oceanography*, *25*, 1333–1349, 1995.

Chalikov, D. and Belevich, M. One-dimensional theory of the wave boundary layer, *Boundary-Layer Meteorology*, *63*, 65–96, 1993.

Chao, Y.Y., Burroughs, L.D. and Tolman, H.L. Wave forecasting for western North Atlantic and adjacent waters., *NOAA/NWS Technical Bulletin*, *459*, 1999.

Chawla, A. and Tolman, H.L. Automated grid generation for WAVEWATCH III. Tech. Note 254, *Tech. rep.*, 2007.

Chawla, A. and Tolman, H.L. Obstruction Grids for Spectral Wave Models, *Ocean Modelling*, *22*, 12–25, 2008.

Collard, F., Ardhuin, F. and Chapron, B. Persistency of ocean swell fields observed from space, *Journal of Geophysical Research*, pp. 1–11, 2008.

Cotton, P.D. and Carter, D.J.T. Cross calibration of TOPEX, ERS-1, and GEOSAT wave heights, *Journal of Geophysical Research*, *99*, 25,025–25,033, 1994.

Durrant, T.H. and Greenslade, D.J.M. Spatial Evaluations of ACCESS Marine Surface Winds using Scatterometer Data, *Australian Meteorological and Oceanographic Journal - Submittted*.

Durrant, T.H., Greenslade, D.J.M. and Simmonds, I. Validation of Jason-1 and Envisat Remotely Sensed Wave Heights, *Journal of Atmospheric and Oceanic Technology*, *26*, 123, 2009a.

Durrant, T.H., Greenslade, D.J.M. and Warren, G.R. Assessing Upgrades to the Bureau of Meteorology's Wave Forecasting System using Satellite Altimeter Data, *CAWCR Technical Report*, 2009b.

Durrant, T.H., Woodcock, F. and Greenslade, D.J.M. Consensus Forecasts of Modeled Wave Parameters, *Weather and Forecasting*, *24*, 492, 2009c.

Glahn, H.R. and Ruth, D.P. The New Digital Forecast Database of the National Weather Service, *Bulletin of the American Meteorological Society*, *84*, 195, 2003.

Greenslade, D.J.M. *Upgrades to the Bureau of Meteorology's Ocean Wave Forecasting System*, 2000.

Greenslade, D.J.M. The assimilation of ERS-2 significant wave height data in the Australian region, *Journal of Marine Systems*, *28*, 141–160, 2001.

Greenslade, D.J.M. Marine Forecasting at the Bureau of Meteorology, in *The Past, Present and Future of Numerical Modelling - Sixteeth annual BMRC Modelling Workshop*, vol. 54, p. 113, 2004.

Greenslade, D.J.M. and Young, I.R. The impact of altimeter sampling patterns on estimates of background errors in a global wave model, *Journal of Atmospheric & Ocean Science*, *22*, 1895–1917, 2005a.

Greenslade, D.J.M., and Young, I.R. The impact of inhomogenous background errors on a global wave data assimilation system, *Journal of Atmospheric and Ocean Science*, *10*, 61–93, 2005b.

Greenslade, D.J.M., Schulz, E.W. Kepert, J.D. and Warren, G.R. The impact of the assimilation of scatterometer winds on surface wind and wave forecasts, *Journal of Atmospheric and Ocean Science*, *10*, 261–287, 2005.

Hanson, J. and Jensen, R. Wave system diagnostics for numerical wave models, in *8 th International Workshop on Wave Hindcasting and Forecasting, Oahu, Hawaii, November*, pp. 231–238, 2004.

Hardy, T. A wave model for the Great Barrier Reef, *Ocean Engineering*, *28*, 45–70, 2001.

Hasselmann, K. et al. Measurements of wind-wave growth and swell decay during the Joint North Sea Wave Project (JONSWAP), *Ergnzungsheft zur Deutschen Hydrographischen Zeitschrift Reihe*, *8*, 1973.

Hess, G.D., Colman, R.A. and McAvaney, B.J. On computing screen temperatures, humidities and anemometer-height winds in large-scale models, *Aust. Met. Mag*, *44*, 139–145, 1995.

Holthuijsen, L., Booij, N. Ris, R. Haagsma, I.G. Kieftenburg, A. and Kriezi, E.E. SWAN Cycle III version 40.11 user manual, *Delft University of Technology, The Netherlands*, 2002.

Hubert, W.E. A preliminary report on numerical sea condition forecasts, *Monthly Weather Review*, *85*, 200–204, 1957.

Janssen, P. Quasi-linear Theory of Wind-Wave Generation Applied to Wave Forecasting, *Journal of Physical Oceanography*, *21*, 1631–1642, 1991.

Janssen, P., Doyle, J.D. Bidlot, J. Hansen, B. Isaksen, L. and Viterbo, P. Impact and Feedback of Ocean Waves on the Atmosphere, in *Advances in Fluid Mechanics*, edited by W.Perrie, vol. 1, chap. Atmosphere, pp. 155–197, 2002.

Janssen, P.A.E.M. Progress in ocean wave forecasting, *Tech. rep.*, ECMWF, 2007.

Janssen, P.A.E.M. Progress in ocean wave forecasting, *Journal of Computational Physics*, *227*, 3572–3594, 2008.

Kepert, J.D., Greenslade, D.J.M. and Hess, G.D. Assessing and Improving the Marine Surface Winds in the Bureau of Meteorology Numerical Weather Prediction Systems, *BMRC Research Report*, 2005.

Komen, G.J., Hasselmann, S. and Hasselmann, K. On the Existence of a Fully Developed Wind-Sea Spectrum, *Journal of Physical Oceanography*, *14*, 1271–1285, 1984.

Leeuwenburg, T. Introducing the Natural Language Generation of Text Weather Forecasts in the GFE, *CAWCR Research Letters*, *July*, 2009.

Leonard, B. A stable and accurate convective modelling procedure based on quadratic upstream interpolation, *Computer methods in applied mechanics and engineering*, *19*, 59–98, 1979.

Leonard, B. The ULTIMATE conservative difference scheme applied to unsteady one-dimensional advection, *Computer methods in applied mechanics and engineering*, *88*, 17–74, 1991.

Lionello, P., Gunther, H. and Janssen, P. Assimilation of altimeter data in a global third-generation wave model, *Journal of Geophysical Research*, *97*, 14,453, 1992.

Mackay, E.B.L., Retzler, C.H., Challenor, P.G. and Gommenginger, C.P. A parametric model for ocean wave period from Ku band altimeter data, *Journal of Geophysical Research*, *113*, 1–16, 2008.

Menard, Y., Fu, L.L., Escudier, P., Parisot, F., Perbos, J., Vincent, P., Desai, S., Haines, B. and Kunstmann, G. The Jason-1 Mission, *Marine Geodesy*, *26*, 131–146, 2003.

NGDC. 2-minute gridded global relief data (ETOPO2), 2006.

NMOC. Implementation of WAM wave model, *Operations Bulletin*, 1994.

NMOC. Changes to the Operational Sea State Forecast System, *Tech. rep.*, Bureau of Meteorology, 2002.

NMOC. Operational implementation of the ACCESS Numerical Weather Prediction systems, *Operations Bulletin*, pp. 1–35, 2010.

NRL. Digital bathymetry data base 2-minute resolution v. 3 (DBB2)., 2006.

Petkovic, P. and Buchanan, C. Australian Bathymetry and Topography Grid [Digital Dataset], *Geoscience Australia, Canberra*, 2002.

Puri, K., Dietachmayer, G.S., Mills, G.A., Davidson, N.E., Bowen, R.A. and Logan, L.W. The new BMRC Limited Area Prediction System, LAPS, *Aust. Meteor. Mag*, *47*, 203–223, 1998.

Rawlins, F., Ballard, S., Bovis, K., Clayton, A., Li, D., Inverarity, G., Lorenc, A. and Payne, T. The Met Office global four-dimensional variational data assimilation scheme, *Quarterly Journal of the Royal Meteorological Society*, *133*, 347–362, 2007.

Resti, A., Benveniste, J., Roca, M., Levrini, G. and Johannessen, J. The Envisat Radar Altimeter System(RA-2), *ESA Bulletin*, *98*, 94–101, 1999.

Rogers, W. The U.S. Navy's Global Wind-Wave Models: An Investigation into Sources of Errors in Low-Frequency Energy Predictions, *Naval Research Lab Tech Report*, 2002.

Rogers, W.E., Wittmann, P.A., Wang, D.W.C., Clancy, R.M. and Hsu, Y.L. Evaluations of global wave prediction at the fleet numerical meteorology and oceanography center, *Weather and Forecasting*, *20*, 745–760, 2005.

Schulz, E., Kepert, J. and Greenslade, D. An Assessment of Marine Surface Winds from the Australian Bureau of Meteorology Numerical Weather Prediction Systems, *Weather and Forecasting*, *22*, 613–636, 2007.

Seaman, R., Bourke, W., Steinle, P., Hart, T., Embery, G., Naughton, M. and Rikus, L. Evolution of the Bureau of Meteorology's Global Assimilation and Prediction system. Part 1: Analysis and initialisation, *Aust. Meteor. Mag*, *44*, 1–18, 1995.

Smith, W. and Sandwell, D. Global sea floor topography from satellite altimetry and ship depth soundings, *Science*, *277*, 1956, 1997.

Snyder, R.L., Dobson, F.W., Elliott, J.A. and Long, R.B. Array measurements of atmospheric pressure fluctuations above surface gravity waves, *Journal of Fluid Mechanics Digital Archive*, *102*, 1–59, 1981.

Sverdrup, H.U. and Munk, W.H. *Wind, Sea and Swell: Theory of Relations for Forecasting*, 1947.

Taylor, K. Summarizing multiple aspects of model performance in a single diagram, *J. Geophys. Res*, *106*, 7183–7192, 2001.

Tolman, H. Effects of Numerics on the Physics in a Third-Generation Wind-Wave Model, *Journal of Physical Oceanography*, *22*, 1095–1111, 1992.

Tolman, H. On the selection of propagation schemes for a spectral wind-wave model, *NWS/NCEP Office Note*, *411*, 30, 1995.

Tolman, H. and Chalikov, D. Source Terms in a Third-Generation Wind Wave Model, *Journal of Physical Oceanography*, *26*, 2497–2518, 1996.

Tolman, H., Balasubramaniyan, B., Burroughs, L.D., Chalikov, D.V., Chao, Y.Y., Chen, H.S. and Gerald, V.M. Development and implementation of wind-generated ocean surface wave models at NCEP, *Weather and Forecasting*, *17*, 311–333, 2002.

Tolman, H. L., Alleviating the Garden Sprinkler Effect in wind wave models, *Ocean Modelling,* 4, 269–289, 2002b.

Tolman, H. Treatment of unresolved islands and ice in wind wave models, *Ocean Modelling*, *5*, 219–231, 2003.

Tolman, H. A mosaic approach to wind wave modeling, *Ocean Modelling*, *25*, 35–47, 2008.

Tolman, H. User manual and system documentation of WAVEWATCH III TM version 3.14, *Tech. rep.*, Tech. Rep. 276, NOAA/NWS/NCEP/MMAB, 2009.

Treloar, A. QNH Derivation and Forecasting in the GFE, *CAWCR Research Letters*, December, 2009.

WAMDIG. et al. The WAM model - A third generation ocean wave prediction model, *J. Phys. Oceanogr*, *18*, 1775–1810, 1988.

Wessel, P. and Smith, W.H.F. A global, self-consistent, hierarchical, high-resolution shoreline database, *Journal of Geophysical Research*, *101*, 8741–8743, 1996.

Wittmann, P. and O'Reilly, W. WAM Validation of Pacific Swell, in *5th International Workshop on Wave Hindcasting and Forecasting*, pp. 83–87, 1998.

Woodcock, F. and Engel, C. Operational consensus forecasts, *Weather and forecasting*, *20*, 101–111, 2005.

Young, I.R. and Vledder, G.P.V. A Review of the Central Role of Nonlinear Interactions in Wind-Wave Evolution, *Philosophical Transactions: Physical Sciences and Engineering*, *342*, 505–524, 1993.

APPENDIX A. BUOY DETAILS

Table A.1 Wave buoys located around the Australian coast. Those used for verification are shown in bold.

Station No.	Name	Lat.	Lon.	Depth (m)
52121	Weipa	-12.68	141.75	6
55014	Bateman's Bay	-35.71	150.34	73
55017	**Byron Bay**	**-28.69**	**153.73**	**72**
55018	**Coffs Harbour**	**-30.35**	**153.27**	**73**
55019	**Crowdy Head**	**-31.83**	**152.86**	**79**
55020	Eden	-37.29	150.18	110
55022	Port Kembla	-34.48	151.03	78
55024	**Sydney**	**-33.77**	**151.42**	**85**
55026	**Strahan**	**-42.08**	**145.01**	**100**
55028	Cairns	-16.73	145.72	15
55029	Townsville	-19.17	147.05	18
55031	Mackay	-21.03	149.55	29
55032	Hay Point	-21.27	149.32	10
55033	Emu Park	-23.3	151.07	22
55034	Moreton Bay	-27.25	153.2	11
55035	Brisbane	-27.5	153.63	73
55036	Gold Coast	-27.97	153.45	18
55037	Tweed Heads	-28.18	153.58	25
55039	**Kingfish B**	**-38.6**	**148.19**	**78**
55040	**Cape du Couedic**	**-36.07**	**136.62**	**80**
56002	**North Rankin**	**-19.59**	**116.14**	**125**
56004	**Jurien**	**-30.29**	**114.91**	**42**
56005	**Rottnest Island**	**-32.11**	**115.4**	**48**
56006	**Cape Naturaliste**	**-33.36**	**114.78**	**50**
56007	Thevenard	-21.41	114.94	16

APPENDIX B. BUOY TIMESERIES

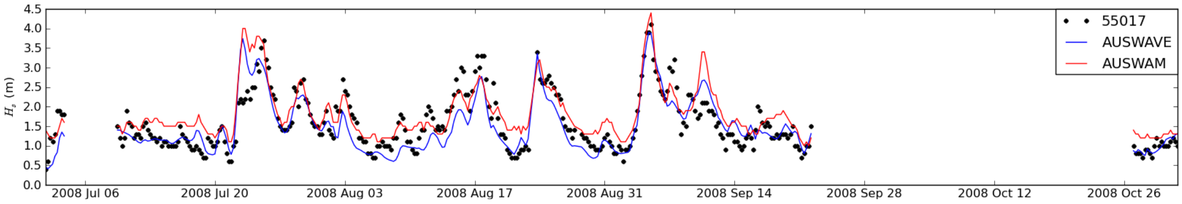

(a) 55017

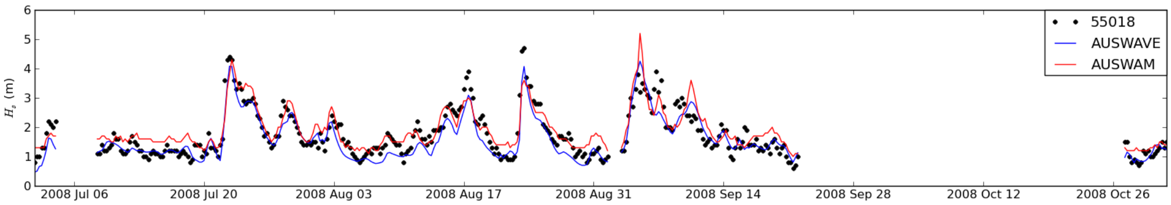

(b) 55018

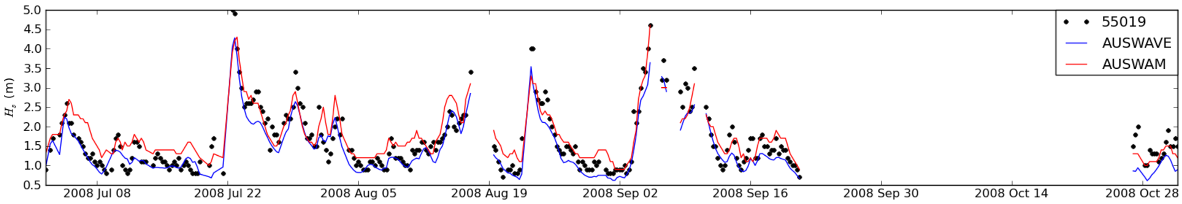

(c) 55019

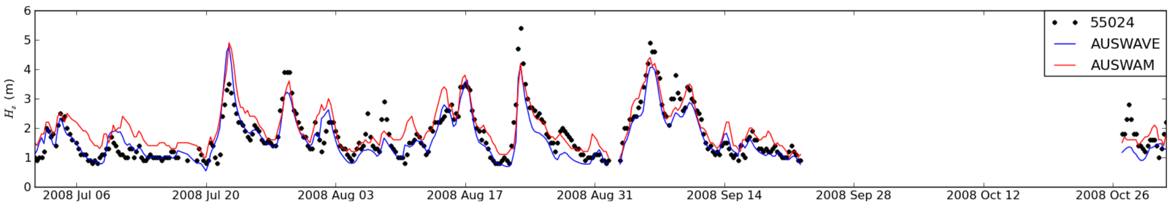

(d) 55024

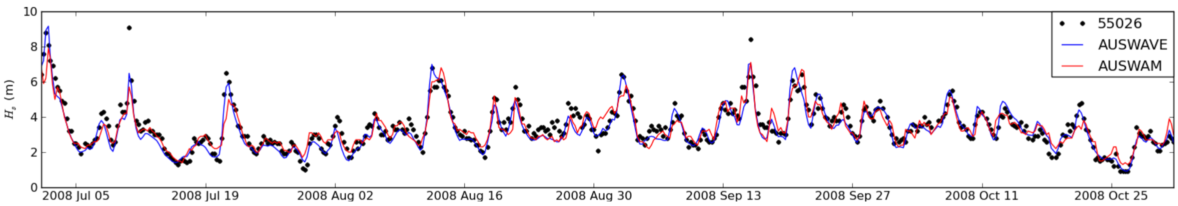

(e) 55026

Fig.B.1   Buoy and model time series for the entire study period

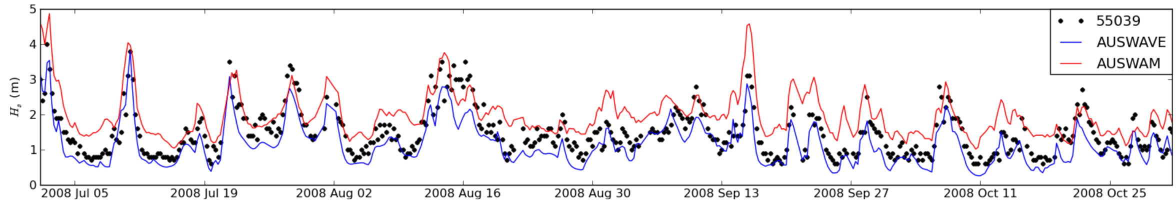

(a) 55039

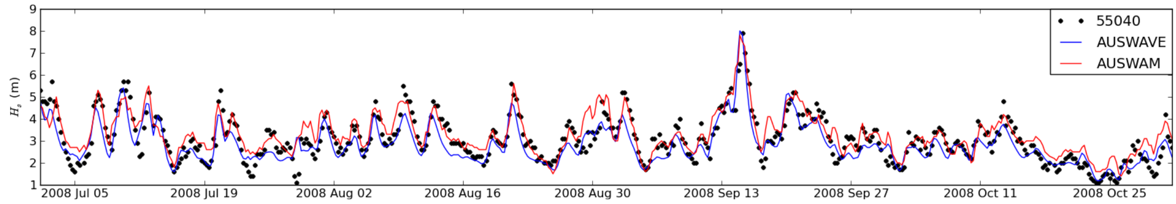

(b) 55040

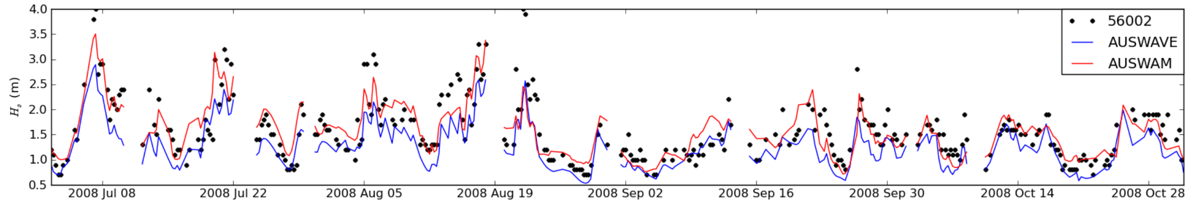

(c) 56002

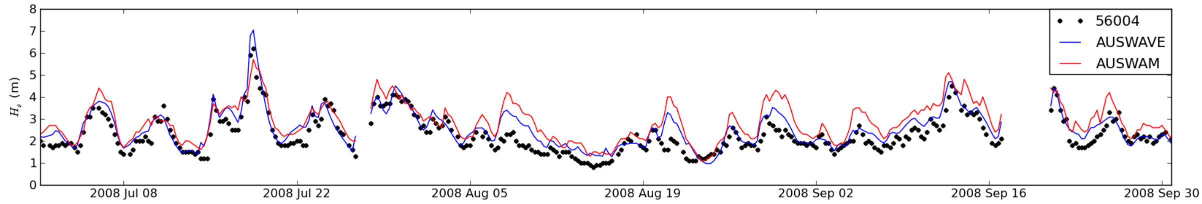

(d) 56004

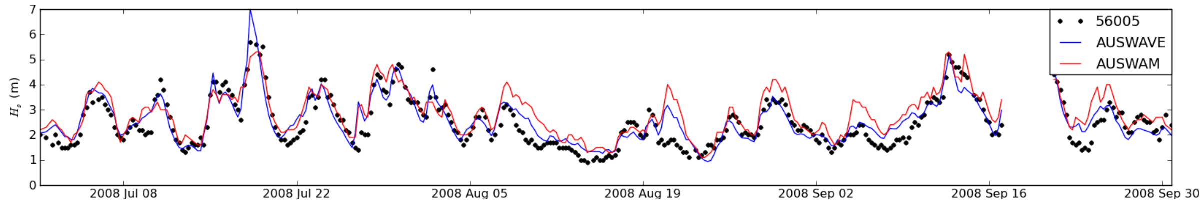

(e) 56005

Fig.B.2 Buoy and model time series for the entire study period (cont.)

APPENDIX C. SPECTRAL PARTITIONING WITHIN AUSWAVE

As it currently stands, the Bureau's main marine forecast product consists of a total wave height, as well as wave heights associated with both wind sea and swell. To produce these products, forecasters are heavily reliant on the partitioning done within the operational forecast models. The way that this partitioning is done has changed significantly with the transition from AUSWAM to AUSWAVE. This Appendix contains some discussion of the practical implications of this change.

The process of spectral partitioning attempts to separate the spectrum into distinct wave systems such as locally growing wind seas and swells that have propagated from elsewhere. This process is not straightforward. Indeed, agreement about how wind sea and swell is defined in general can be hard to reach, with definitions between the modelling community and forecasters often varying, and a certain amount of subjectivity coming to bear.

Wind waves are generally described with an energy density spectrum. An example of such a spectrum in given in Fig. C.1. On the left, polar direction shows the direction in which the waves propagate, with frequency indicated by radial distance from the centre. This example shows a spectrum with two clearly identifiable peaks, indicating two separate wave systems, the broad wind sea peak propagating to the NW and a narrow swell peak propagating to the NE. Integrating over directions gives the energy density as a function of frequency only, presented on the right. This is quite a simple example, and in general, the existence of several swell systems make the appropriate partitioning less obvious.

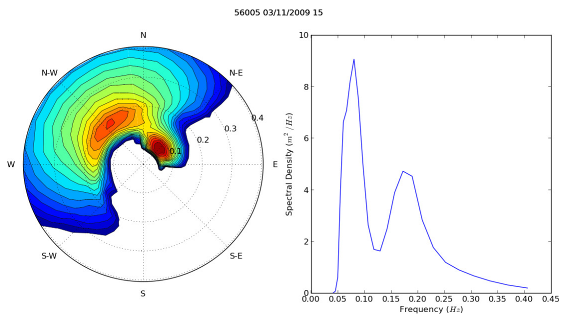

Fig.C.1 Example spectrum, represented as a polar plot showing spectral energy density in both frequency and directional space on the left, and integrated over direction on the right.

Wind sea/swell partitioning in WAM relies on a reasonably simple relationship between the wind speed and the wave phase speed given by:

$$c_p > \sqrt{0.9 + 0.07 u_{10}}\, u_{10} \cos(\theta - \theta_{wind}) \qquad \text{(C.1)}$$

where c_p is the wave phase speed, θ is direction of travel of the wave component and θ_{wind} is the direction of the forcing wind. In essence, wind sea is defined as that part of the spectrum which is being actively forced by the wind. The remaining spectrum defines the swell.

There are major limitations to this method of separation. While it can be argued that this technique does a reasonable job of separating the wind sea component, averaging what remains into a single swell component is clearly insufficient when the swell component consists of multiple wave systems, as is usually the case. The resultant output swell will more than likely indicate a fictitious swell that is the average of multiple systems.

These deficiencies have been addressed in the latest release of WW3, which now uses a more sophisticated scheme, based on the work of *Hanson and Jensen* (2004), applying the watershed algorithm of Vincent1991. In its original form, this algorithm was used to determine peaks and valleys on a contour plot, and predict the flow of water as it fell on mountain ranges. When applied to the inverted wave spectrum, the individual wave systems can be extracted. A similar approach to that used by WAM in terms of wind speed and wave phase speed relations is then applied to each wave system to assign a wind sea/swell fraction. The process can be summarised by the following steps:

1. Determine partitions (using the Vincent1991 watershed algorithm)
2. Determine the wind sea fraction for each partition (the fraction of the partition that is being actively forced)
3. Combine all partitions with a wind sea fraction bigger than a set threshold value to give the wind sea partition.
4. Rank the remaining partitions by the total energy in each, and assign as primary swell, secondary swell etc.

Under this scheme, an arbitrary number of individual wave systems, or spectral partitions, can be identified. Parameters for each spectral partition can then be calculated as described in *Hanson and Jensen* (2004).

Further details of this approach can be found in the papers mentioned above. In practice, the biggest change is that instead of outputting a single wind sea and a single swell, as was the case with AUSWAM, AUSWAVE finds the wind-sea and all the swell systems that are present, which is an arbitrary number. The number of swell systems that are actually output is pre-determined. If there are more swell systems present than have been defined, then the remaining systems are ignored. This partitioning is done at every grid point, producing gridded outputs of these fields. Figure C.2 shows some example spectral output products from the Bureau's product viewer[5].

While this approach is undoubtedly more physically meaningful, it does present some problems with the forecast process as it currently stands, particularly within GFE. Perhaps greatest of these is the fact that that gridded partition data contains gaps. For the wind sea grids, this occurs when no partition satisfies the minimum wind sea fraction that is required in order to be defined as wind sea. In this case, all partitions will appear as a swell. In the case of the swell grids, for the primary swell, a gap means that all of the energy has been assigned as wind sea. This usually occurs under strong winds, when growing seas dominate the spectrum. For the secondary swell, it means that there are less than three distinct wave groups present (one wind sea and two swells). In the example above, this can be readily seen in the case of the strong winds to the south of Tasmania. Under the area of maximum winds, a large portion of the spectrum is being forced, and hence is assigned to wind sea. Behind the storm, as the generated waves move away from the storm, they are assigned to the swell partitions.

[5]http://www.bom.gov.au/australia/charts/viewer/index.shtml?domain=combinedW\&type=sigWaveHgt

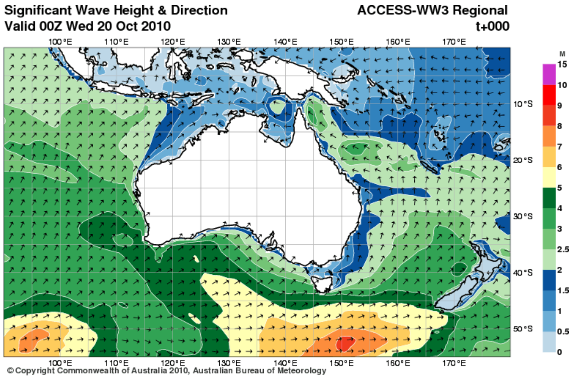

(a) Total H_s

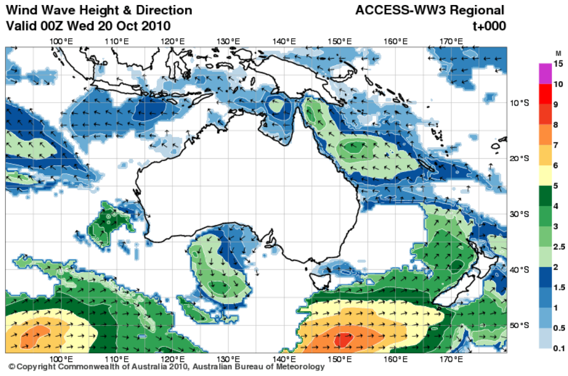

(b) Wind Sea

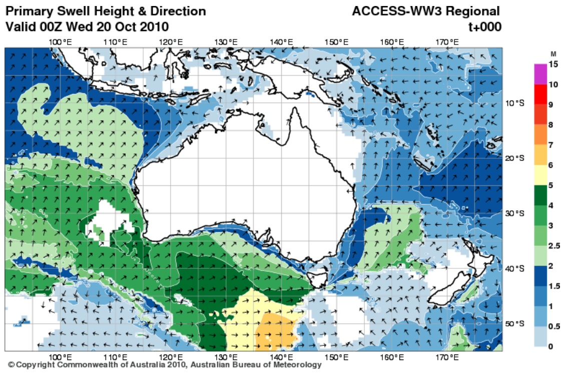

(c) Primary Swell

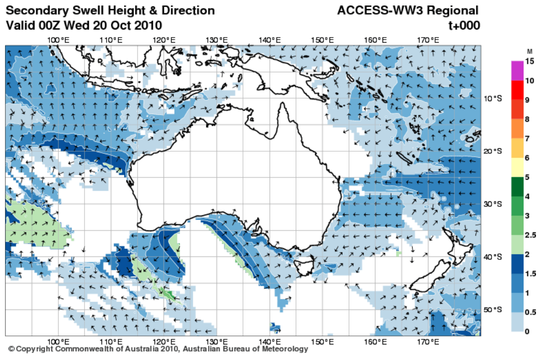

(d) Secondary Swell

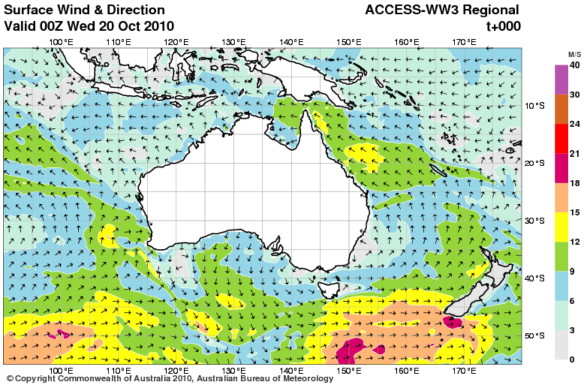

(e) Wind Speed

Fig.C.2 Examples of partitioned data.

the wind sea grids, this occurs when no partition satisfies the minimum wind sea fraction that is required in order to be defined as wind sea. In this case, all partitions will appear as a swell. In the case of the swell grids, for the primary swell, a gap means that all of the energy has been assigned as wind sea. This usually occurs under strong winds, when growing seas dominate the spectrum. For the secondary swell, it means that there are less than three distinct wave groups present (one wind sea and two swells). In the example above, this can be readily seen in the case of the strong winds to the south of Tasmania. Under the area of maximum winds, a large portion of the spectrum is being forced, and hence is assigned to wind sea. Behind the storm, as the generated waves move away from the storm, they are assigned to the swell partitions.

Looking at the fields above, there appears to be a lack of spatial consistency for the swell fields. For example, in the Bight, it is obvious that when all the fields are added up, they are consistent with the total Hs, however, the separation seems haphazard, with little spatial consistency within the allocations. It is important to realise that the partitioning is done at each grid point individually, without reference to its neighbours. Hence, under stronger winds in the Bight, one of the partitions is classified as wind sea. As waves propagate away from this system, they appear as swell. However, another swell already exists in the region, as seen in the primary swell, so this energy appears in the secondary swell. As the wave systems propagate from grid point to grid point, the local ranking of that wave system may change, and hence it is reallocated from primary swell to secondary swell.

The Centre for Australian Weather and Climate Research is a partnership between CSIRO and the Bureau of Meteorology.